REALIZATION OF VIRTUAL FLUID ENVIRONMENT ON A ROBOTIC GAIT TRAINER FOR THERAPEUTIC PURPOSES

A THESIS SUBMITTED TO
THE GRADUATE SCHOOL OF NATURAL AND APPLIED SCIENCES
OF
THE MIDDLE EAST TECHNICAL UNIVERSITY

BY

TAYFUN EFE ERTOP

IN PARTIAL FULFILLMENT OF THE REQUIREMENTS
FOR
THE DEGREE OF MASTER OF SCIENCE
IN
MECHANICAL ENGINEERING

JUNE 2017

Approval of the thesis:

REALIZATION OF VIRTUAL FLUID ENVIRONMENT ON A ROBOTIC GAIT TRAINER FOR THERAPEUTIC PURPOSES

Submitted by **TAYFUN EFE ERTOP** in partial fulfillment of the requirements for the degree of **Master of Science in Mechanical Engineering Department, Middle East Technical University** by,

Prof. Dr. Gülbin Dural Ünver
Dean, **Graduate School of Natural and Applied Sciences** _____

Prof. Dr. Raif Tuna Balkan
Head of Department, **Mechanical Eng.** _____

Assoc. Prof. Dr. Erhan ilhan Konukseven
Supervisor, **Mechanical Eng. Dept., METU** _____

Assist. Prof. Dr. Ahmet Buğra Koku
Co-supervisor, **Mechanical Eng. Dept., METU** _____

Examining Committee Members:

Assoc. Prof. Dr. Yiğit Yazıcıoğlu
Mechanical Eng. Dept., Middle East Technical University _____

Assoc. Prof. Dr. Erhan ilhan Konukseven
Mechanical Eng. Dept., Middle East Technical University _____

Assist. Prof. Dr. Ahmet Buğra Koku
Mechanical Eng. Dept., Middle East Technical University _____

Assist. Prof. Dr. Ali Emre Turgut
Mechanical Eng. Dept., Middle East Technical University _____

Assist. Prof. Dr. Kutluk Bilge Arıkan
Mechatronics Eng. Dept., Atılım University _____

Date: 14.06.2017

I hereby declare that all information in this document has been obtained and presented in accordance with academic rules and ethical conduct. I also declare that, as required by these rules and conduct, I have fully cited and referenced all material and results that are not original to this work.

Name, Last name: Tayfun Efe Ertop

Signature: _____

ABSTRACT

REALIZATION OF VIRTUAL FLUID ENVIRONMENT ON A ROBOTIC GAIT TRAINER FOR THERAPEUTIC PURPOSES

Ertop, Tayfun Efe

MSc., Department of Mechanical Engineering

Supervisor: Assoc. Prof. Dr. Erhan ilhan Konukseven

Co-supervisor: Assist. Prof. Dr. Ahmet Buğra Koku

June 2017, 75 pages

Patients with disorders such as spinal cord injury, cerebral palsy and stroke can perform full gait when assisted, which progressively helps them regain the ability to walk. A very common way to create assistive effects is aquatic therapy. Aquatic environment also creates resistive effects desired for increasing muscle activity. Simulating the fluid environment using a robotic system would enable therapists to adjust various fluid parameters so that the therapy is tailored to each patient's unique state. In this study, realization of a virtual fluid environment on a robotic gait trainer for rehabilitation purposes is presented. A model is created to determine torques and forces exerted on a partially submerged human body by the fluid environment. Then, the fluid model is used to create a control scheme which is implemented on a robotic gait trainer. A compensation algorithm is developed so that weight and friction of robotic links are countered. Smooth transition between stance and swing phases of gait is ensured with a developed algorithm that only uses kinematic data. Experiments with healthy subjects were done to verify the stance-swing algorithm, the changes in gait characteristics between land and water conditions, and to assess effects of changes in fluid model parameters to gait characteristics. It is shown that realization of virtual

fluid environment on robotic gait trainer is achieved. The torque measurements showed that the controller was able to make the orthosis transparent to the patient. Significant changes in gait characteristic were observed by modifying fluid model parameters.

Keywords: Robotic Rehabilitation, Robotic Gait Trainer, Medical Robotics, Locomotor Therapy, Aquatic Rehabilitation Therapy

ÖZ

AKIŞKAN ORTAMLARIN REHABİLİTASYON AMACI İLE ROBOTİK YÜRÜYÜŞ SİSTEMİ ÜZERİNDE GERÇEKLENMESİ

Ertop, Tayfun Efe
Yüksek Lisans, Makina Mühendisliği Bölümü
Tez Yöneticisi: Doç. Dr. Erhan ilhan Konukseven
Ortak Tez Yöneticisi: Yrd. Doç. Dr. Ahmet Buğra Koku

Haziran 2017, 75 sayfa

Omurilik hasarı, serebral palsi veya inme gibi sağlık sorunlarına sahip hastalar fiziksel olarak desteklendikleri zaman yürüyebilmektedirler. Bu durum zaman içinde yürüme yeteneklerini geri kazanmalarına yardım etmektedir. Yürüyüş sırasındaki destek etkilerini yaratmak için çok sık kullanılan yöntemlerden biri akuatik rehabilitasyondur. Akuatik ortam aynı zamanda kas gelişimine yardım edecek şekilde hastalara direnç göstermektedir. Akışkan ortamın bir robotik system üzerinde gerçeklenmesi fizyoterapistlerin çeşitli akışkan parametrelerini değiştirerek terapiyi her hastanın özel durumuna göre ayarlayabilmesine imkan verecektir. Bu çalışmada, akışkan ortamlar rehabilitasyon amacı ile robotik yürüyüş sistemleri üzerinde gerçeklenmiştir. Kısmi olarak suya daldırılmış insan vücudu üzerine akışkan ortam tarafından etki eden kuvvet ve torkları hesaplamak için bir model geliştirilmiştir. Daha sonra bu model bir kontrol altyapısı oluşturulmak için kullanıldı ve oluşturulan bu kontrol altyapısı bir robotik yürüyüş cihazına uygulandı. Robotik sistemin parçalarının ağırlık ve sürtünme etkilerine karşı koyacak bir dengeleme algoritması geliştirildi. Yürüyüşün duruş fazı ve sallanma fazı arasında yumuşak bir geçiş olması için sadece vücut parçalarının kinematik verilerini kullanan bir algoritma geliştirildi. Sağlıklı bireylerle robotik

yürüyüş cihazı ile yapılan deneylerle duruş-sallanma faz algoritması ve kara ve su ortamlarında oluşan yürüyüş karakteri farklılıkları doğrulandı, ve akışkan model parametrelerinde yapılan değişikliklerin yürüyüş karakterine olan etkileri değerlendirildi. Elde edilen sonuçlarla sanal akışkan ortamların robotik yürüyüş cihazları üzerinde gerçeklenebildiği gösterildi. Yapılan tork ölçümleri kontrol altyapısının robot parçalarını robota bağlı kullanıcıya hissettirmediğini göstermiştir. Akışkan modelin parametrelerinde yapılan değişikliklerin yürüyüş karakterinde önemli değişikliklere neden olduğu görülmüştür.

Anahtar Sözcükler: Robotik Rehabilitasyon, Robotik Yürüme Cihazı, Medikal Robotlar, Lokomotor Terapi, Akuatik Rehabilitasyon

To

My dear family…

Those who battle to overcome their disabilities…

ACKNOWLEDGMENTS

First of all, I would like to express my gratitude to my supervisor Assoc. Prof. Dr. Erhan ilhan Konukseven and co-supervisor Asst. Prof. Dr. Ahmet Buğra Koku for their invaluable support and guidance.

Besides my supervisors, I would like to thank Prof. Dr. Erbil Dursun, DPT, for his inputs regarding rehabilitation methods used in practice and Assoc. Prof. Dr. M. Metin Yavuz for his advices regarding fluid environment modeling.

I would like to thank BAMA Technology (METU Technopark, Turkey) for supporting this study. Special thanks are due to Murat Topçu (CEO), Can Mehmet Ali Çiftçi (Chief R&D Manager), Dilay Kayiş, Tolga Uzun, Kıvılcım Çakır, Eren Deniz Çelebi and rest of the R&D team. Their support and collaboration made this study possible.

I would also like to thank METU Biomechanics Lab for their support regarding reference healthy gait data utilized in computer simulations.

I am deeply grateful to my colleague Tolga Yüksel for his assistance and collaboration during this entire study. I would also like to thank all my METU Mechanical Engineering Department colleagues Sedat Pala, Sinan Özgün Demir, Onurcan Kaya, Musab Çağrı Uğurlu, Uğur Mengilli, Ata Jafari, İsmail Özçil, Berke Harmancı and Abdülhamit Dönder for their support.

I would like to thank my parents, Hüseyin Ertop and Hanım Sağıroğlu, for their endless support and understanding. Also, I would like express my gratitude to Damla Dağ for her continuous support and encouragement during this study.

Lastly, I would like to thank the Scientific and Technological Research Council of Turkey (TUBITAK) for their financial support with grant code BIDED2210 during my graduate education.

TABLE OF CONTENTS

ABSTRACT v

ÖZ vii

DEDICATION ix

ACKNOWLEDGMENTS x

TABLE OF CONTENTS xii

LIST OF TABLES xv

LIST OF FIGURES xvi

LIST OF ABBREVIATIONS xix

CHAPTERS

1. INTRODUCTION 1

1.1. Locomotor Training and Aquatic Physical Rehabilitation 1

1.2. Robotic Devices and Rehabilitation 4

1.3. Scope of the Thesis 9

1.4. Outline of the Thesis 10

2. MODELS AND ALGORITHMS DEVELOPED FOR HUMAN GAIT IN FLUID ENVIRONMENT 13

2.1. Modeling of Human Body in Fluid Environment 13

2.1.1. Buoyancy Model 15

2.1.2. Drag Model 16

2.1.3. Loads on Lower Extremity during Support and Swing Phases 17
2.2. Support and Swing Transition Algorithm 18
2.3. Summary 21
3. COMPUTER SIMULATIONS 23
3.1. Buoyancy and Drag Model Simulations 24
3.2. Single Lower Extremity Simulations 25
3.3. Support and Swing Transition Algorithm Simulations 27
3.4. Full Gait Simulations 29
3.5. Summary 30
4. IMPLIMENTATION TO ROBOTIC GAIT TRAINER 33
4.1. RoboGait: The Robotic Gait Trainer Used 33
4.2. Weight and Friction Compensation Model for Robotic Orthosis System 34
4.3. Overall Control Scheme 36
4.4. Experiments to Verify the Gravity and Friction Compensation Model 37
4.5. Summary 39
5. EXPERIMENTS WITH HEALTHY SUBJECTS 41
5.1. Single Lower Extremity Experiments 41
5.2. Experiments for Complete Gait 44
5.2.1. Stance and Swing Transition Algorithm Experiments 46
5.2.2. Land vs Water Experiments 47
5.2.3. Experiments with Varied Drag Coefficient, Fluid Density and Fluid Level 49
5.2.4. Flow Experiments 52
5.3. Summary 54
6. CONCLUSION & FUTURE WORK 55

6.1. Conclusion 55
6.2. Future Work 57
REFERENCES 59
APPENDICES 67
A. PSEUDOCODES FOR COMPUTER SIMULATIONS 67
B. THE EXPERIMENTAL FLOW USED FOR COMPLETE GAIT EXPERIMENTS 71

LIST OF TABLES

TABLES

Table 1. Joint torques on lower extremities and their equivalents in the annotation. 18

Table 2. Means (±SD) of temporal and spatial gait parameters of the healthy subjects' gait cycles (N=850) for land and water walking conditions with RoboGait..... 49

Table 3. Means (±SD) of temporal and spatial gait parameters of the healthy subjects' gait cycles (N=700) for four different fluid model parameter sets with RoboGait. Only one parameter is changed in each parameter set with respect to Base Case (refer to the table)..... 52

Table 4. Means (±SD) of temporal and spatial gait parameters of the healthy subjects' gait cycles (N=700) for different flow velocities (refer to the table) with RoboGait. 54

LIST OF FIGURES

FIGURES

Figure 1. Locomotor training sessions with (a) elderly subjects [6],and (b) children [7] 2

Figure 2. Aquatic training sessions (a) alone [23], and (b) with a therapist [9]..... 3

Figure 3. Aquatic treadmill devices: (a) HydroWorx 1000^{TM} [29], [31], and (b) Flow Mill [11] 4

Figure 4. Examples of upper extremity robotic rehabilitation devices. (a) patient cooperative control based ARMin robot [33], (b) wrist rehabilitation robot [38], and (c) arm exoskeleton L-Exos [35]..... 5

Figure 5. Examples of robotic gait trainers. (a) Lokomat [44], and (b) RoboGait [52] 7

Figure 6. Examples of lower extremity exoskeletons. (a) BLEEX [57], (b) SUBAR [64], and (c) underwater gait assist robot [66] 8

Figure 7. Representation of (a) the enumeration of body parts and their lengths (b) buoyancy and drag forces on different body segments of human body walking at velocity $\vec{v}_{body}$ against a flow with velocity $\vec{v}_{flow}$ where fluid level is h_f 14

Figure 8. An example of notations used for body segment *i*..... 15

Figure 9. Representation of strip theory..... 16

Figure 10. Flow chart of the stance and swing transition algorithm developed 20

Figure 11. Eqn. 2.11 plotted in [0.0, 1.0] range 20

Figure 12. Drag Simulation Results 24

Figure 13. Buoyancy and drag torque outputs of the fluid model obtained during the single lower extremity computer simulations for hip extension exercise 26

Figure 14. A picture of the created real time animation based on computer simulations 27

Figure 15. Weighting factors, α_R and α_L, calculated for right and left lower extremities, respectively, during the full gait computer simulations 28

Figure 16. Joint angles, and buoyancy and drag torque outputs of the fluid model for the full gait computer simulations 30

Figure 17. Picture of RoboGait with its labeled subsystems 34

Figure 18. Actuator, load cell and mechanical link arrangements for RoboGait's orthosis system 35

Figure 19. Diagram of control scheme used for the overall system 37

Figure 20. Load cell and actuator arrangement for hip joint 38

Figure 21. Torques expected due to fluid model and actual measured torques 38

Figure 22. Effects of adjustable parameters on buoyancy and drag torque outputs of the model for hip extension exercise with single lower extremity 43

Figure 23. A picture taken during one of the experiment sessions with the healthy subjects 45

Figure 24. Outputs of the support and swing transition algorithm for +0.8 km/h walking speed of healthy subjects in land walking conditions with RoboGait 47

Figure 25. Mean hip and knee angles and angular velocities of the healthy subjects' gait cycles (N=850) for land and water walking conditions with RoboGait..... 48

Figure 26. Mean values of angles, and applied drag and buoyancy torques for hip and knee joints during the healthy subjects' gait cycles (N=700) with four different fluid model parameter sets (refer to the legend of figure) on RoboGait..... 50

Figure 27. Mean values of angles, angular velocities and drag torques for hip and knee joints during the healthy subjects' gait cycles (N=700) with different flow velocities (refer to legend of the figure) on RoboGait..... 53

LIST OF ABBREVIATIONS

ROM	Range of Motion
EMG	Electromyography
GRF	Ground Reaction Force
AAN	Assist-as-needed
DS	Double Support
SCI	Spinal Cord Injury
DOF	Degree of Freedom
VR	Virtual Reality
FES	Functional Electrical Stimulation
BW	Body Weight
LL	Leg Length
SD	Standard Deviation

CHAPTER 1

INTRODUCTION

This chapter includes a review of the literature regarding this study, explanation about the scope and objectives of the thesis, and the outline for the forthcoming chapters of the thesis.

1.1. Locomotor Training and Aquatic Physical Rehabilitation

Gait rehabilitation methods aim to help patients with locomotor dysfunction in lower extremities due to conditions like spinal cord injury (SCI), cerebral palsy and stroke perform gait exercise so that the walking ability can be restored. Through proper rehabilitative treatment, it is proven that motor functions can be restored to some extent [1], [2]. Different methodologies are used to tackle this problem. One of the earliest solutions was manually assisted treadmill training, locomotor training, in which more than one therapist moves patient's legs by hand as shown in Figure 1. Physical activity is especially essential for functional improvement during the early stages of the injury whilst neural plasticity is present [3]. Improvements in ambulation abilities of patients who received locomotor training are proven with randomized clinical trials [4]–[6].

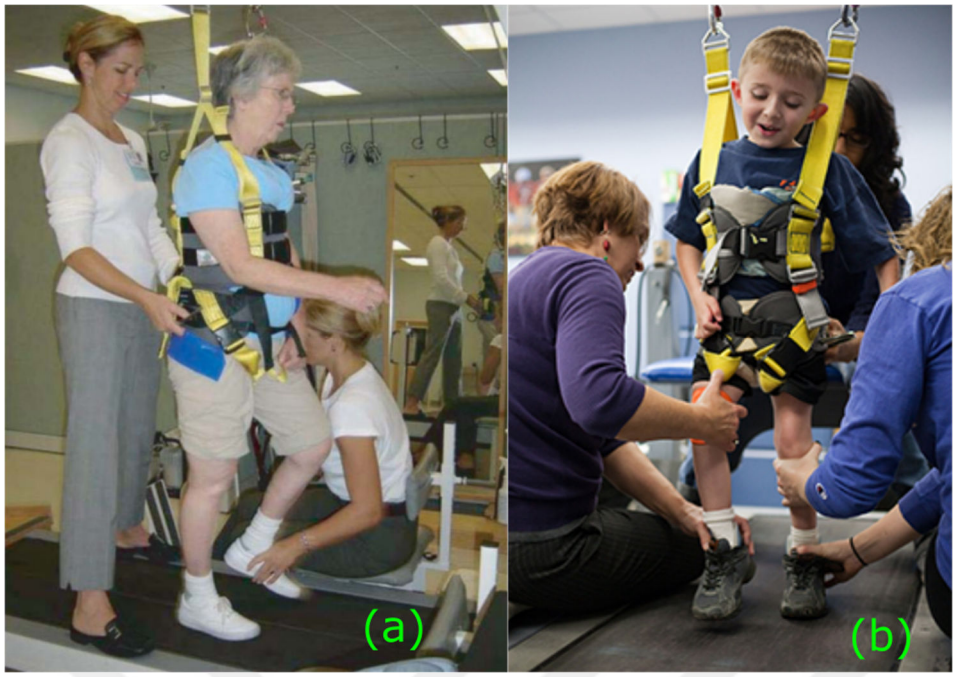

Figure 1. Locomotor training sessions with (a) elderly subjects [6],and (b) children [7]

Labor intensive nature of the original locomotor training forced researchers to seek for alternative methods. One of the viable options is considered to be aquatic physical therapy. Example aquatic therapy sessions are shown in Figure 2. Aim of aquatic rehabilitation is to improve the strength and stability of movements, and range of motion (ROM). Aquatic environment is preferred for its buoyancy and drag effects. Water can provide safe environment for patients to walk without the fear of falling meanwhile buoyancy effects both assist their lower extremity and decrease the apparent weight [8]. Patients can even walk in water although they are not able to walk on land [9]. Drag forces, on the other hand, create the necessary resistive forces to promote muscle development. Muscle activity during aquatic training is demonstrated in detail by previous studies [10]–[13]. Although their adjustability is very limited, tools like buoyancy cuffs and hydro boots can be used to alter the drag and buoyancy characteristics of aquatic therapy [14], [15]. Chest-high water reduces body weight carried by the patient by %65 [8]. Being in water also relaxes patients and increases their blood circulation [16]. In aquatic therapy, patients are free to initiate the movement of their limbs and they are not forced to follow any pre-defined movement patterns. Albeit underwater therapy has these advantages, it has some challenges

during treatment sessions which cannot be overlooked. Water temperature is needed to be controlled during sessions for the relaxation effect and a therapist is generally need to assist the patient for the whole session. Clinical studies showed that aquatic training programs improves patients' walking function and postural balance [17]–[20]. Other clinical studies showed increased neuromuscular performance in subjects after aquatic training [21], [22].

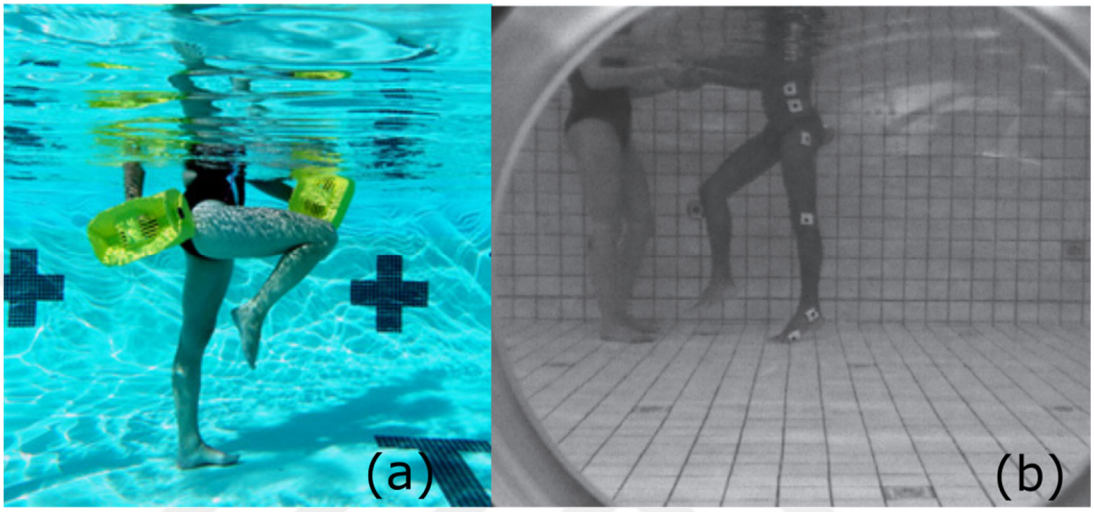

Figure 2. Aquatic training sessions (a) alone [23], and (b) with a therapist [9]

Easier-to-use alternatives are underwater treadmill devices. These devices require much less space. Examples of aquatic treadmill devices are displayed in Figure 3. Reduced metabolic expenditure during aquatic treadmill training compared to overground treadmill training is proven by Jung et al. which allows therapists to prolong the therapy sessions for post-stroke patients [24]. Randomized clinical studies verify improved neuromuscular performance at lower extremity after aquatic treadmill training exercise [25]–[27]. Clinical studies also show improved walking ability and balance in patients who received aquatic treadmill training [26]–[28]. Being able to use water jets to create more resistance, especially for the sports injury treatments, is also another reason to use these devices over pools [29]. Also, additional weights can applied to limbs of the subjects to increase resistance effects [30].

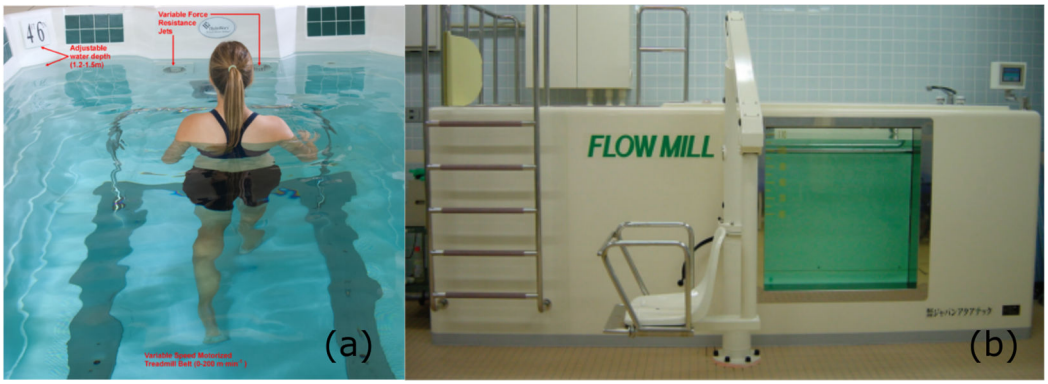

Figure 3. Aquatic treadmill devices: (a) HydroWorx 1000^{TM} [29], [31], and (b) Flow Mill [11]

1.2. Robotic Devices and Rehabilitation

Usage of robotic devices for rehabilitation practices is expanding progressively each day. Robotic rehabilitation devices are also considered to be a viable option for undertaking the heavy labor required during physical therapy sessions. Dynamic reactions and controllability of robotic systems makes them favorable over the conventional rehabilitation methods. The number of academic studies regarding this topic is rapidly increasing [32].

Human body has a large number of degree of freedoms (DOF) and high power demands on most of these joints [8]. Therefore, designing robotic systems that are compatible with human body is quite a challenging engineering problem. Work done in this flied is mainly focused on extremities of human body, namely upper extremity (including arms and hands) and lower extremity (including thighs, legs and feet). This is due to the fact that manipulation of objects and walking have a very significant role in everyday life.

Upper extremity rehabilitation mainly aims to enhance the coordination of upper extremity motions and improve the motor function. One study focuses on using a patient cooperative control based robotic system to guide the patient's arm in 3D space while an audiovisual feedback is being used to motivate the patient through different tasks [33]. Similar studies use virtual reality (VR) environment set up to simulate everyday tasks on robotic systems connected the patients' upper extremity [34], [35].

Another study uses a robotic orthosis to diagnose abnormalities present at patient's upper extremities and the therapy is shaped to improve the functionality at the problematic joints [36]. In addition, several studies target restoring wrist and hand functions using robotic systems [37]–[40]. Examples of upper extremity rehabilitation robots are presented in Figure 4.

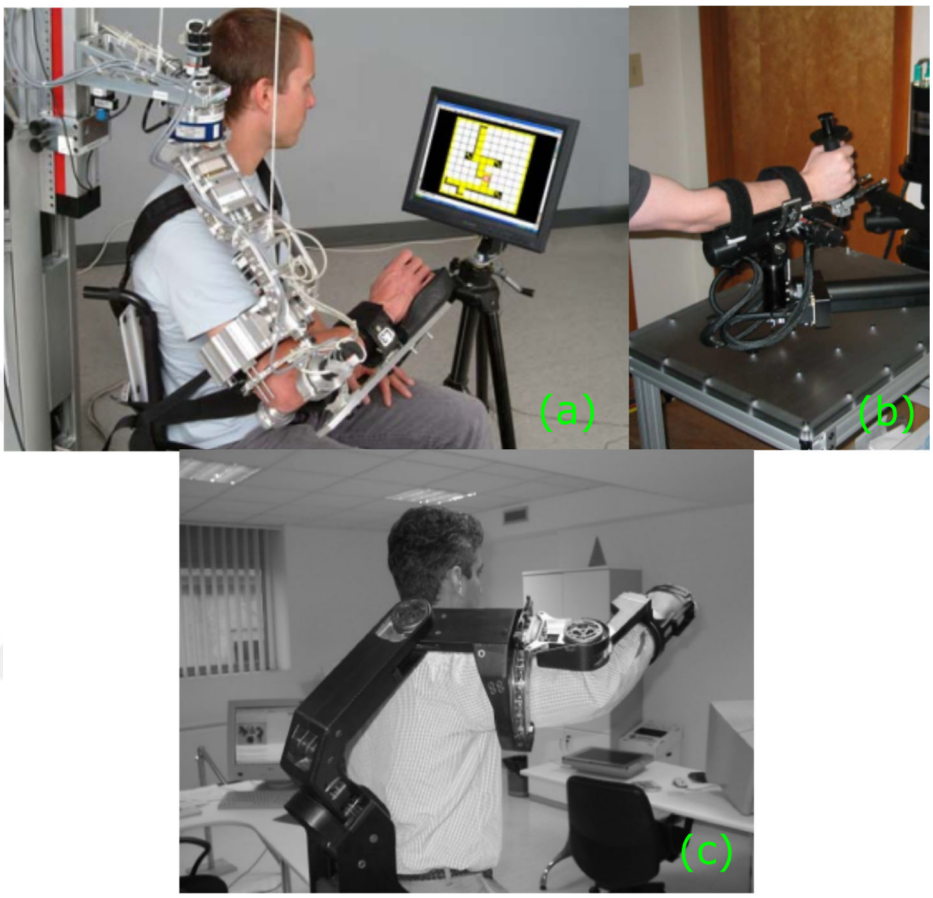

Figure 4. Examples of upper extremity robotic rehabilitation devices. (a) patient cooperative control based ARMin robot [33], (b) wrist rehabilitation robot [38], and (c) arm exoskeleton L-Exos [35]

As for the lower extremity, robotic gait trainers are widely used in physical rehabilitation centers and hospitals to help SCI, cerebral palsy and stroke patients. Using robotic gait trainers is another alternative for the conventional locomotor training. Labor is transferred to robotic systems, and duration and intensity of the therapy sessions are, therefore, increased. Outcomes of clinical study [41] imply that increased intensity of rehabilitation sessions would improve the functional recovery. This result promotes the usage of robotic gait trainers. Intense labor demand of the

locomotor training may also jeopardizes the accuracy of repeated movement patterns inflicted on patients [42]. Robotic gait trainers, on the other hand, are capable of repeating the same pattern over and over without any deviations. Robotic systems are quite suited for performing this type of repetitive tasks. Robotic gait trainers have the ability to support the desired fraction of the patient's weight. Patients are helped to follow a predefined gait pattern on a treadmill by the forces applied to their legs using the robotic orthosis. Robotic gait trainers make use of orthosis systems with actuators to actively guide the patient into the desired gait pattern [43]–[46]. Randomized clinical studies with robotic gait trainers showed functional improvements in patients [47]. Assistive and strict control modes are utilized on robotic gait trainers in practice. The control approach used in a robotic gait trainer is quite decisive due to the fact that it directly changes characteristic of the therapy. Classic position control methods can be used if strict pattern following is desired. In such cases patient does not need to utilize any motor skills. Unlike classical methods, assist-as-needed (AAN) control schemes are designed to favor the muscle activity and to yield some flexibility. Admittance or impedance control to make the robotic trainer behave compliant [44] and control strategies involving a band of error tolerance around a movement pattern [45], [46] are among AAN control strategies. Another approach is to tackle AAN paradigm as an optimization problem [48], [49]. The common downside of these studies is the requirement for a reference movement pattern. The same reference pattern is, then, imposed on all patients during therapy with limited tuning capability. Using audiovisual data to motivate patients to perform exercises can be considered another control methodology utilized on robotic gait trainers. The subjects were reported to be more motivated and concentrated on their exercise with a robotic gait trainer in the presence of a visual feedback [50]. In another study, VR environment is implemented in a robotic gait trainer so that patients can practice crossing various obstacles created in the VR environment [51]. Some examples of robotic gait trainers are shown in Figure 5.

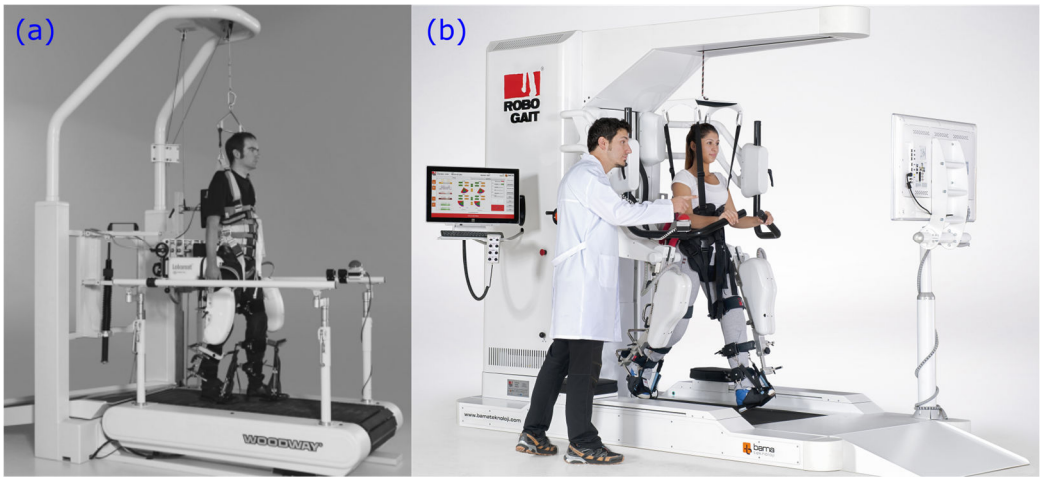

Figure 5. Examples of robotic gait trainers. (a) Lokomat [44], and (b) RoboGait [52]

Robotic exoskeletons are another type of robotic devices that are used for lower extremity rehabilitation. Portability of exoskeletons is an important advantage over other robotic systems with larger and heavier setups. Lower extremity exoskeletons provide more mobility for patients and can be integrated in everyday life of the patients rather than being able to be used during limited durations of therapy sessions only. One simple approach is to use a passive exoskeleton system to counter balance the gravity effects of the lower extremity as presented in [53]. Another robotic exoskeleton system is ALEX which utilizes an ANN methodology [54]. ALEX creates a force field in the tunnel around the desired gait pattern and helps the patients to walk by applying forces determined this field. Impedance control strategies that consist of utilizing virtual springs, dampers and inertias are also utilized for robotic rehabilitation as a part of ANN methodology [55], [56]. On the other hand, exoskeleton system BLEEX shown in Figure 6-a uses inverse dynamics of the robotic system for a positive feedback controller [57]. Another approach is to use muscle activity to determine robotic system outputs. One study focuses on synchronizing the torque outputs of exoskeleton actuators to real time muscle activity [58]. Another study, on the other hand, focuses on implementing a hybrid control approach that uses both robotic systems and functional electrical stimulation (FES) of patients' muscles [59]. Some other studies focus on adapting different types actuators such as pneumatic actuators and soft actuators to exoskeletons [60], [61]. While most studies concentrate on joint-

by-joint control, some studies explore sub-task level control strategies and try to assist sub-tasks involved in gait such as foot clearance, balance and etc. [62]. Furthermore, a different study focuses on assessing and dampening the tremors occurring in patients' body [63] which is quite distinctive from common motion assisting behaviors implemented on robotic exoskeletons.

Another study that is also inspired by aquatic environment involves creating a non-strict control algorithm for walking in a exoskeleton shown in Figure 6-b [64], [65]. That study concentrates on modelling gait in stagnant water environment alone while a scaling factor of 0.3 is used to limit assistive effect of buoyancy forces. Other fluid environments and effects of fluid parameters like density, drag coefficient or flow velocity were not investigated. There are also robotic exoskeleton systems that operate under water, shown in Figure 6-c, which help patients to perform gait in such an environment [66]. However, these devices are limited to utilizing only water.

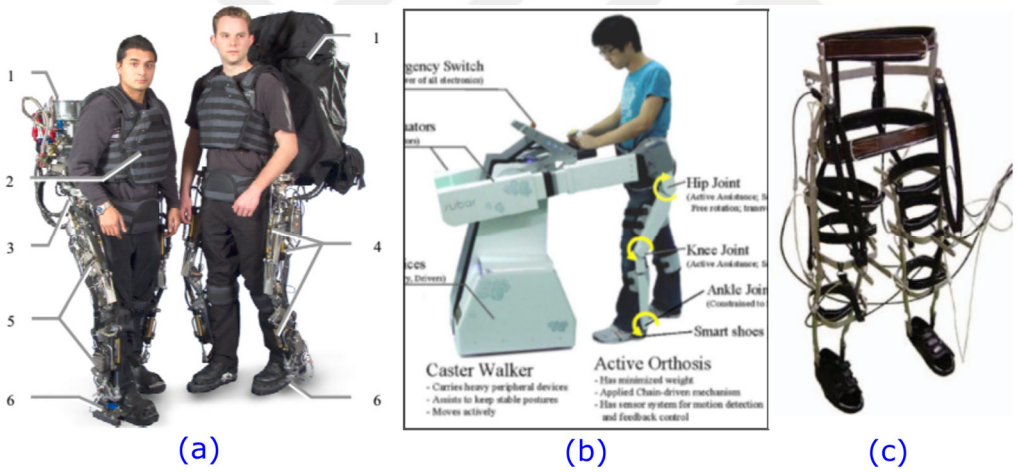

Figure 6. Examples of lower extremity exoskeletons. (a) BLEEX [57], (b) SUBAR [64], and (c) underwater gait assist robot [66]

Apart from robotic gait trainers and robotic exoskeletons, other types of robotic devices used for lower extremity rehabilitation includes robotic fitness devices. One example for such device would be MoreGait device which provides a feasible rehabilitation opportunity at home for prolonged therapy duration [67]. MoreGait device has two pneumatic actuators at each joint which work in an antagonistic arrangement to supply sensory stimuli to lower extremity of patients. Antigravity

treadmills can also be considered among such devices. Antigravity treadmill devices utilize inflatable chambers and seals to reduce apparent body weight of the subject. It has been shown that knee forces can be reduced significantly with antigravity treadmills [68]. Yet another such robotic device is Andago (Hocoma AG, Switzerland) [69]. Andago is a cutting edge robotic device that targets close the gap between treadmill based exercises and free walking. Andago has a dynamic body weight support system on a wheeled platform which actively follows patients while they perform upright and free gait in a safe environment.

1.3. Scope of the Thesis

In short, aquatic therapy has the advantage of being completely patient driven while assisting locomotion in different ways, whereas robotic therapy has the edge when it comes to adjustability. Both of these advantages can be kept for rehabilitation purposes if water therapy is simulated on a robotic gait trainer. The weight off-loading system and the robotic orthosis of robotic gait trainers can be used to simulate the drag and buoyancy forces acting on the body parts while the treadmill system is being utilized to facilitate walking. Since all fluid parameters in such a therapy would be virtual, the range of their values have no physical limitations. Therefore, apart from water, fluids which do not exist but could be very suitable for a patient's rehabilitation can be applied to that patient during therapy. As stated in [70], human body will make every attempt to conserve energy during gait and development of gait pattern is by natural experimentation starting from childhood. With the developed method in this study, any suitable fluid environment can be simulated to enable patients with walking disability go through the same natural experimentation process. This kind of a control method would behave passively and encourage patients to initiate movement by themselves, unlike conventional control methods used in robotic gait trainers. This new method does not impose any pre-defined patterns on the patient whereas common robotic rehabilitation methods in literature generally enforce pre-defined patterns. Another advantage of this new method is that robotic systems are more accessible and easier to maintain compared to pools or other underwater therapy devices. Therefore,

it has a potential to become a feasible alternative for creating conventional aquatic therapy effects on even remote and small rehabilitation centers.

In this study, a control system that realizes human gait in virtual fluid environment was developed on robotic gait trainer. A model for calculating fluid forces and torques on a lower extremity moving in a fluid environment was developed for complete gait. Accuracy of the model is checked using computer simulations. Outputs of these simulations were compared with the results of previous experimental studies. A control structure is created based on the developed model and it is implemented on a robotic gait trainer. Another model for determining and counter balancing the torques created by the weight and friction of robotic links was also included in the control structure. Effectiveness of the controller in compensating the weight and friction effects is evaluated with experiments. A hip extension exercise used in aquatic therapy was performed with the robotic system while varying drag coefficient, fluid density and flow velocity, and the data collected was presented. The developed fluid model requires the stance swing phase information of each lower extremity for complete gait analysis. For this purpose, a phase detection algorithm that only utilizes online kinematic gait data was proposed. The proposed algorithm was tested against actual gait phase data obtained from experiments with healthy subjects. Experiments were also done with healthy subjects to evaluate the extended fluid model for complete gait and effects of changing its parameters. Comparisons between land and water walking conditions, various flow velocity conditions, and conditions with changed fluid parameters (fluid density, drag coefficient and fluid level) were made. Algorithms that realize these functions are developed and tested on a robotic system called RoboGait (Bama Technology, Turkey) [52].

1.4. Outline of the Thesis

In Chapter 2, modelling of fluid forces and torques acting on human body during gait in a fluid environment and a developed algorithm for smooth gait phase transition are presented. The fluid model includes drag and buoyancy effects. The developed gait phase transition algorithm utilizes the kinematic data of limbs.

In Chapter 3, the computer simulations based on the fluid model and the developed support and swing transition algorithm are presented. The fluid model simulations are compared with previous experimental studies in literature. Single lower extremity and full gait simulations are performed to examine the calculated loads on human joints.

In Chapter 4, implementation of the fluid model and the gait phase transition algorithm on a robotic gait trainer is presented. Weight and friction compensation model used for robotic links is explained and its effectiveness is tested with experiments. Overall control structure used is discussed in detail.

In Chapter 5, the results of the experiments performed with healthy subjects on the robotic gait trainer are presented. Changes in the fluid model torque and force outputs, and gait characteristics of the healthy subjects are discussed for various virtual fluid environment cases along with the gait phase transition algorithm results.

Chapter 6 includes conclusions driven from this work and suggestions regarding prospective studies.

CHAPTER 2

MODELS AND ALGORITHMS DEVELOPED FOR HUMAN GAIT IN FLUID ENVIRONMENT

In this chapter, the fluid model created for forces and torques acting on human body in fluid environment is presented along with the developed stance and swing phase transition algorithm.

2.1. Modeling of Human Body in Fluid Environment

Human body is assumed to be performing gait while being partially immersed in fluid environment for the model. Human body is divided into five rigid body segments (legs, thighs and upper-body) connected by hip and knee joints which are treated as revolute joints. The lower extremity body segments are modeled as truncated cone shaped bodies. For the upper-body segment, cylinders are utilized for head and arms whereas a rectangular prism is used for torso. While determining the dimensions for rigid body segments from actual subjects, measurement methodologies explained in [71] are utilized. Ankle joints are not used for body part segmentation in the scope of this study. Feet are included in leg body segments. The reason for that is the proposed methodology is aimed to be implemented on already existing robotic gait trainers in the market and these robotic systems do not have actuators for the ankle joints. Also, according to [72] ankle joint's major role during forward gait is providing support to the body rather than push the body forward. Buoyancy forces in fluid environment decreases the body weight supported and, thus, diminishes the need for the ankle joints

to provide support [8]. In this study, buoyancy forces for overall body is applied by weight-off loading system of robotic gait trainers decreasing the apparent body weight supported by the subject. Therefore, even without ankle actuators the major fluid effects are recreated at ankle joints. For a new robotic system with ankle joint actuation, the same modeling methodology can easily be implemented by including ankle joints at body part segmentation process.

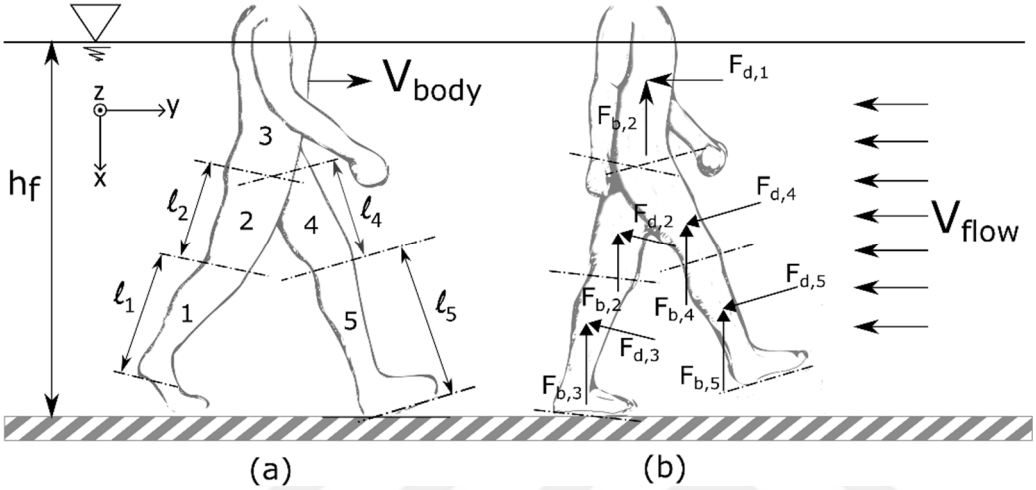

Figure 7. Representation of (a) the enumeration of body parts and their lengths (b) buoyancy and drag forces on different body segments of human body walking at velocity $\vec{v}_{body}$ against a flow with velocity $\vec{v}_{flow}$ where fluid level is h_f.

For this study, upper body is assumed to be moving with a constant gait velocity, $\vec{v}_{body}$, as shown in Figure 7. Velocity, $\vec{v}_i$, at any point on i^{th} lower extremity segment can be calculated by kinematic equation as,

$$\vec{v}_i(\ell) = \vec{v}_{i-1,i} + \vec{\omega}_i \times \vec{r}_i(\ell) \tag{2.1}$$

where $\vec{v}_{i-1,i}$ is linear velocity of proximal joint of the segment, $\vec{\omega}_i$ is angular velocity of the segment and $\vec{r}_i$ is position vector of the point measured from proximal joint which is a function of distance ℓ on the longitudinal axis of segment. Figure 8 below shows the general notations used for the right lower extremity leg segment as an example.

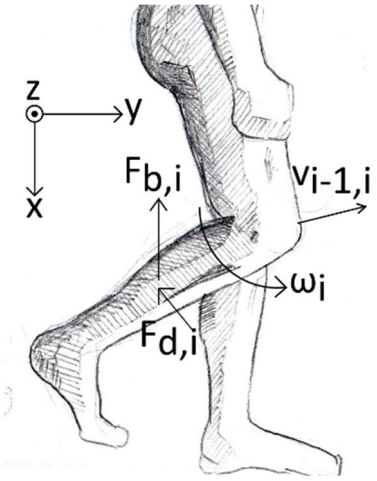

Figure 8. An example of notations used for body segment *i*

Fluid used in the model is assumed to be incompressible and uniform. Forces exerted on a moving object in a fluid can be analyzed under buoyancy, drag and lift. Only buoyancy and drag, as shown in Figure 8 and Figure 7, are taken into account for the fluid model in this study. Since all body segments are selected symmetric in the model, flow around these segments will also be symmetric. Thus, lift coefficient is taken to be zero for all segments.

2.1.1. Buoyancy Model

Buoyancy force is taken to be acting on the volumetric center of each segment and its magnitude equals to weight of the displaced fluid. Direction of buoyant force is always upwards, in –x direction (Figure 8).

Buoyancy force, $\vec{F}_{b,i}$, and moment it creates on the proximal joint, $\vec{\tau}_{b,i}$, for body segment *i* are given by,

$$\vec{F}_{b,i} = -\vec{i}\,\rho_f g V_i \tag{2.2}$$

$$\vec{\tau}_{b,i} = \vec{r}_{vc,i} \times \vec{F}_{b,i} \tag{2.3}$$

where ρ_f is density of fluid, g is gravitational acceleration, V_i is volume of the segment inside the fluid and $\vec{i}$ is unit vector in +x direction. Vector $\vec{r}_{vc,i}$ in Eqn. 2.3 is position vector between the volumetric center of segment and proximal joint.

For this work, fluid level, h_f, is selected such that lower extremities are always inside the fluid.

2.1.2. Drag Model

Only pressure drag is considered for this model. Other factors that contribute drag force like skin friction are neglected. In addition, turbulent flow effects on the drag are also neglected. Pressure drag is calculated by using strip theory mentioned in the study of Orselli and Duarte. This approach is proved be a good estimation for drag effects in their study [8].

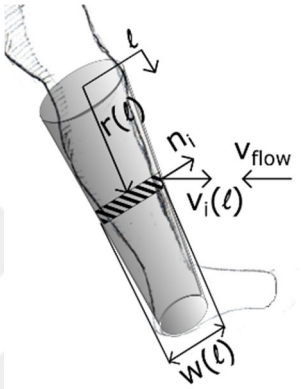

Figure 9. Representation of strip theory

Pressure drag on each differential strip along longitude axis of the body segment as shown in Figure 9. Fluid is assumed to be flowing with a velocity, $\vec{v}_{flow}$. Relative velocity between any point on the body segment and fluid, $\vec{v}_i'$, is found by Eqn. 2.4.

$$\vec{v}_i'(\ell) = \vec{v}_i(\ell) - \vec{v}_{flow} \tag{2.4}$$

While calculating drag effects, frontal area of strips which are perpendicular to relative velocity vector should be used (Figure 9). Drag force, $\vec{F}_{d,i}$, and moment it creates on the proximal joint, $\vec{\tau}_{d,i}$, for body segment *i* are given by,

$$\vec{F}_{d,i} = -\int_0^{L_i} \frac{1}{2} C_D \rho_f w(\ell) \left|\vec{n}_i \bullet \vec{v}_i'(\ell)\right| \; \vec{v}_i'(\ell) \; d\ell \tag{2.5}$$

$$\vec{\tau}_{d,i} = -\int_0^{L_i} \frac{1}{2} C_D \rho_f w(\ell) |\vec{n}_i \bullet \vec{v}_i'(\ell)| \; [\vec{r}_i(\ell) \times \vec{v}_i'(\ell)] d\ell \tag{2.6}$$

where L_i is length of body segment *i*, $w(\ell)$ is width of strip, $\vec{n}_i$ is unit vector normal to frontal area of strips and C_D is coefficient of drag.

In drag calculations, circular drag coefficient, $C_{D,C}$, and rectangular drag coefficient, $C_{D,R}$, are utilized for circular shaped bodies and rectangular prisms, respectively. In order to have only one adjustable parameter for drag, ratio of 2.5 between drag coefficients of rectangular and circular bodies is used to relate them [73]. $C_{D,R}$ is set to 2.5 times the selected value of $C_{D,C}$. Note that drag effects are created on upper body segment as well since it is taken to be moving with velocity $\vec{v}_{body}$ during gait, unlike the preceding study where upper body was assumed to be stationary.

2.1.3. Loads on Lower Extremity during Support and Swing Phases

Different loads are exerted on each lower extremity during support and swing phases of gait. In swing phase, foot does not contact the ground. Torques and forces due to fluid on each joint on the swinging lower extremity can be determined by the fluid effects on that extremity. However, foot contacts the ground at support phase creating reaction force and moments. Torques and forces due to fluid on each joint on the supporting lower extremity can be calculated by treating swinging lower extremity and upper body as distal body segments. Therefore, keeping leg of the swinging lower extremity as the most distal segment (*i=5*) and leg of the supporting lower extremity as the most proximal segment (*i=1*) body segments are numbered from 1 to 5 as shown in Figure 7. Then, resulting torques, $\vec{\tau}_{f,(i-1),i}$, and forces, $\vec{F}_{f,(i-1),i}$, due to fluid on each joint between segment *i-1* and *i* can be calculated by Eqn. 2.7 and Eqn. 2.8 in a similar manner with [74].

$$\vec{F}_{f,(i-1),i} = \vec{F}_{b,i} + \vec{F}_{d,i} + \vec{F}_{f,i,(i+1)} \tag{2.7}$$

$$\vec{\tau}_{f,(i-1),i} = \vec{\tau}_{b,i} + \vec{\tau}_{d,i} + \vec{\tau}_{f,i,(i+1)} + \vec{r}_i(L_i) \times \vec{F}_{f,i,(i+1)} \quad (2.8)$$

According to this notation, joint torques to be applied due to fluid effects on support and swing extremities are given in Table 1.

Table 1. Joint torques on lower extremities and their equivalents in the annotation

Swinging extremity knee	$\vec{\tau}_{k,sw}$	$\vec{\tau}_{f,4,5}$
Swinging extremity hip	$\vec{\tau}_{h,sw}$	$\vec{\tau}_{f,3,4}$
Supporting extremity hip	$\vec{\tau}_{h,sp}$	$\vec{\tau}_{f,2,3}$
Supporting extremity knee	$\vec{\tau}_{k,sp}$	$\vec{\tau}_{f,1,2}$

2.2. Support and Swing Transition Algorithm

During one gait cycle, each lower extremity changes between swing and support phases. Since torques that needs to be applied depend on the phase of that lower extremity, phases of both lower extremities need to be determined in real time. In addition, transition between phases should be as smooth as possible in order to avoid jerky output torques to be applied to patients.

One method used for this task in literature is utilization of ground reaction force (GRF) measurements [65], [75]. Other methods in literature include utilization of accelerometers [76], gyroscopes [77], [78] and surface electromyography (EMG) sensors [79] attached to body. However, the commercial robotic gait trainer platform to be used during experiments, RoboGait, does not have the hardware capabilities for realization of these methods. Therefore, a new method is developed for determination and transition of phases in this study considering the experimental setup. This method utilizes only heel position data and performs transition between phases according to the proposed algorithm.

In this algorithm, weighting variables between 0.0 and 1.0 are assigned for right and left lower extremities, α_R and α_L respectively. This weighting variables indicate the current phase of the extremity where 1.0 is stance phase and 0.0 is swing phase. During

the phase transition these weights change between 0.0 and 1.0. Note that these weight factors always satisfy the condition in Eqn. 2.9.

$$\alpha_R + \alpha_L = 1.0 \tag{2.9}$$

As the vertical distance of one heel to hip joint reaches to its maximum value during stance phase, the other foot will be swing phase thus its heel to hip distance will be considerably shorter. Utilizing this fact, the algorithm presented extracts phase information from the vertical distances of heels to hip joints which are denoted by x_R and x_L for right and left lower extremities, respectively.

The algorithm expects a phase transition if $x_R \approx x_L$. When this transition is caught, computer stores that distance as L_0. Weights of the right and left extremities changed as distance between the lower heel and L_0 increase by Eqn. 2.10 and Eqn. 2.11.

$$t = 1 - \frac{[L_{ext} - L_{Tol}] - [x_{Low}]}{[L_{ext} - L_{Tol}] - L_0} \tag{2.10}$$

$$\alpha_{Low} = \frac{\exp(t^3) - 1}{\exp(t) - 1} \tag{2.11}$$

where t is normalized distance, L_{ext} is length of lower extremity, L_{Tol} is the tolerance from the bottom, α_{Low} and x_{Low} are the parameters for extremity with lower heel position. When the algorithm does not expect a transition, it simply considers the extremity with lower heel position as support and the other extremity as swing. Note that L_{Tol} is the adjustable parameter of the algorithm. For this study it is taken as $L_{Tol} = 0.01\ L_{ext}$. Weight α on the other lower extremity can be found by Eqn. 2.9. The overall support and swing transition algorithm proposed is presented on the flow chart given in Figure 10.

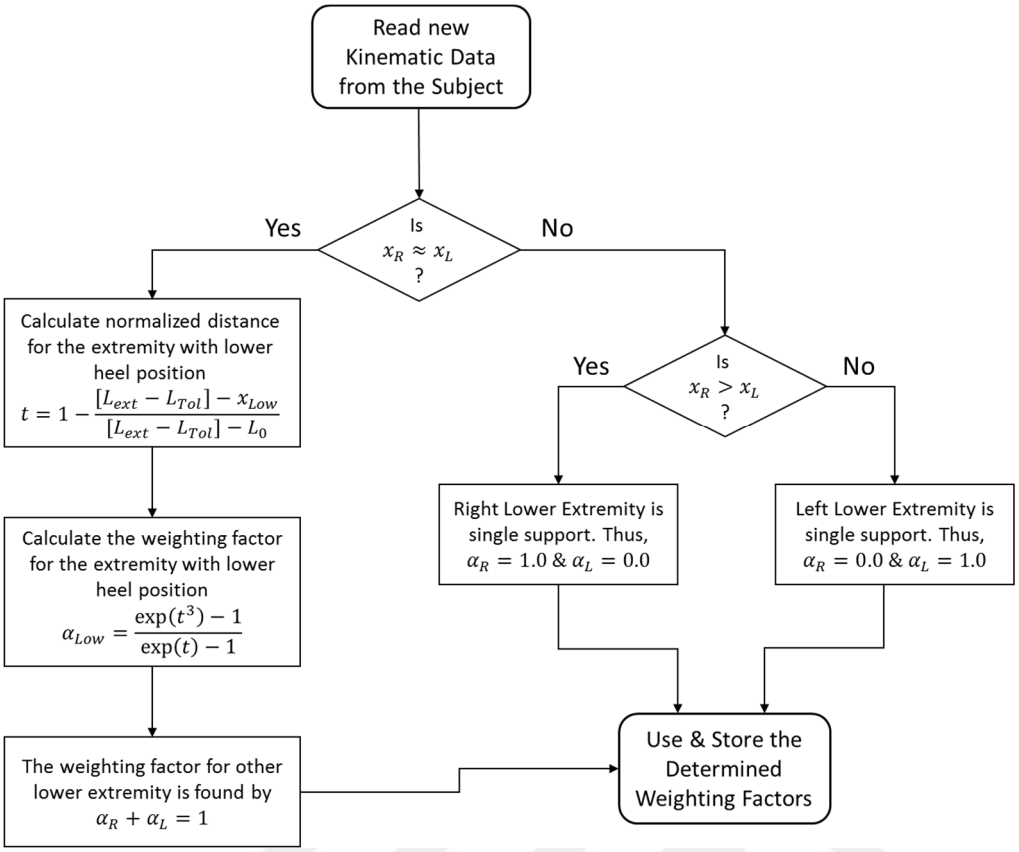

Figure 10. Flow chart of the stance and swing transition algorithm developed

The function in Eqn. 2.11 is selected for transition since fast response is wanted in regions close to $t = 1$. These regions correspond to the end of phase transition where smooth toe-off movement is desired. Figure 11 shows the behavior of the chosen function in [0.0, 1.0] range.

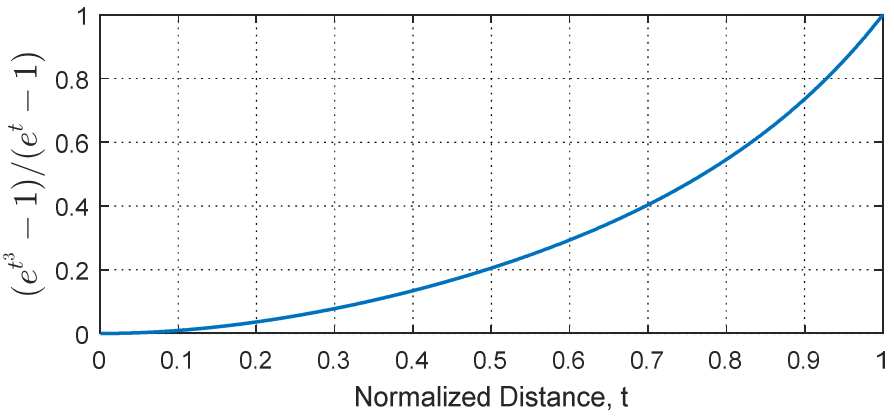

Figure 11. Eqn. 2.11 plotted in [0.0, 1.0] range

Lastly, torques to be exerted due to fluid effects can be calculated with weighing factor. For example, the torque output on the right knee, $[\vec{\tau}_k]_R$, can be found as,

$$[\vec{\tau}_k]_R = \alpha_R [\vec{\tau}_{k,sp}]_R + (1-\alpha_R)[\vec{\tau}_{k,sw}]_R \tag{2.12}$$

where $[\vec{\tau}_{k,sp}]_R$ is the torque value calculated while assuming the right extremity in support phase and $[\vec{\tau}_{k,sw}]_R$ is the torque value calculated while assuming the right extremity in swing phase for knee joint on the right. Torques on the other joints can be found in a similar manner.

2.3. Summary

This chapter covers the developed virtual fluid model for determining fluid torques and forces at human lower extremity joints, and the proposed gait phase detection algorithm for smooth phase transition in detail. Drag and buoyancy were included in the virtual fluid model and lift effects are assumed to be zero. Parameters of the virtual fluid environment such as fluid level, flow velocity, drag coefficient and fluid density were left as adjustable variables so that they can be tuned to manipulate therapeutic effects of the proposed therapy method for each subject. The fluid model yields different torque and force outputs depending on whether the lower extremity is in support or swing phase. Thus, in order to utilize the fluid model during full gait of the subjects, phases of gait for each lower extremity needed to be determined in real time. The proposed gait phase detection algorithm utilizes the kinematic gait data alone to determine the gait phases and to ensure smooth transition between them.

In the following chapter, computer simulations based on the developed fluid model and the proposed support and swing transition algorithm were carried out. Different movement patterns including full gait were utilized in the simulations and the performances of the fluid model and the gait phase transition algorithm were evaluated.

CHAPTER 3

COMPUTER SIMULATIONS

In this chapter, the simulations performed to evaluate the proposed models and algorithms are presented. Buoyancy and drag model outputs are compared with the results of previous experimental studies in the literature. Load exerted on human body due to the fluid environment are explored for two cases, a hip extension exercise performed with a single lower extremity and full gait. Additionally, the stance and swing transition algorithm outputs are assessed during full gait simulations.

For all computer simulations dimensions for body segments were taken from the same average 25-year-old healthy male subject (72 kg body mass and 1.79 m body height) that performed in the single lower extremity experiment and full gait experiments. This was done so that experiments and computer simulations would be based on the same body dimension set and, therefore, have comparable outputs. Most of the previous research and experiments are done using water; thus, for all simulations fluid properties of water were adopted for the fluid model.

Matlab software tool was utilized for all computer simulations. The developed models and algorithms were implemented there as individual standalone functions and called from the main simulation code when required. Pseudocodes for algorithms and models utilized in the computer simulations are provided in Appendix A.

3.1. Buoyancy and Drag Model Simulations

In order to verify the fluid model, buoyancy and drag effects were simulated and compered against data from literature.

Buoyancy model was checked assuming the subject was immersed in chest-high water. Total buoyancy force on the subject's body was calculated and discussed for this condition. For drag model, calculated drag forces acting on leg at different angular speeds were analyzed for different drag coefficients. Other body segments of the subject were taken to be not moving for this analysis and the leg is assumed to be fully immersed into the fluid environment.

Note that density of water is taken as $\rho_f = 998.6 kg/m^3$ and flow velocity is set to zero, $\vec{v}_{flow} = 0 km/h$, for these simulations.

Total buoyancy force on the subject is calculated as 482.2 N from the simulation for chest-high immersion (taken as 1.3m) in water. Total weight of the subject is 706.3 N and this much buoyancy force would decrease body weight supported by the subject to 31.7%. This decrease in body weight is very similar with the values found in literature[8].

Drag simulation results are represented in Figure 12. Magnitude of drag forces with respect to angular speed of the leg around the knee joint were analyzed for three different $C_{D,C}$ values.

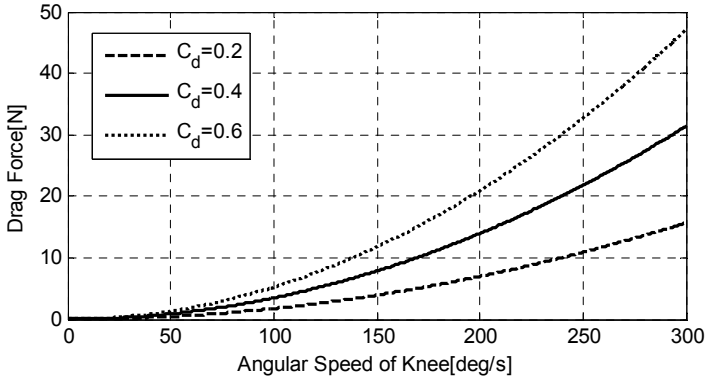

Figure 12. Drag Simulation Results

The results of the simulation were compared to physical experiments done in aquatic environment found in literature. Forces for $C_{D,C} = 0.4$ is found to be comparable with experimental results in [14].

3.2. Single Lower Extremity Simulations

Buoyancy and drag loads on the hip and knee joints of a single lower extremity were determined with computer simulations during a simple hip extension exercise. Hip extension exercise is a commonly used exercise during aquatic therapy sessions in which patients are instructed to perform first extension movement and then flexion movement to the limits with their hip while keeping their knee as straight as possible. The actual angle patterns for joints during this exercise highly depends on the interaction between the patient and fluid environment. Be that as it may, a sinusoidal wave with 2.75 seconds period is used to approximate the hip joint angular patterns during the exercise. Knee joint is assumed to be perfectly straight during whole simulation.

The angular position data used in the simulation is given in Eqn. 3.1 and Eqn. 3.2. Note that θ_h and θ_k are given in degrees.

$$\theta_h = 30\cos\left(\frac{2\pi}{2.75}t\right) \tag{3.1}$$

$$\theta_k = 0 \tag{3.2}$$

Water is selected as the fluid for this simulation. Fluid properties are taken as $\rho_f = 998.6 kg/m^3$, $C_{D,C} = 0.4$ and $h_f = 1.3\,m$ while the flow velocity is kept zero, $\vec{v}_{flow} = 0\,km/h$ [14].

Hip and knee angular positions, angular velocities, and the resulting torques obtained from the simulation are shown in Figure 13. The figure shows that the same torque patterns with different magnitudes for knee and hip were observed for both drag and buoyancy cases. This is due to the perfectly straight knee assumption used for the

simulation which causes two body segments, thigh and leg, to behave as a single rigid body. Notice that the torque behaviors are also the same for hip extension (positive hip angular velocity regions) and hip flexion (negative hip angular velocity regions) portions of the exercise. The reason behind that is the perfectly sinusoidal angle pattern used in the simulations. It should be noted that actual angle patterns during the hip extension exercise may not be identical because of the differences in flexion and extension characteristics.

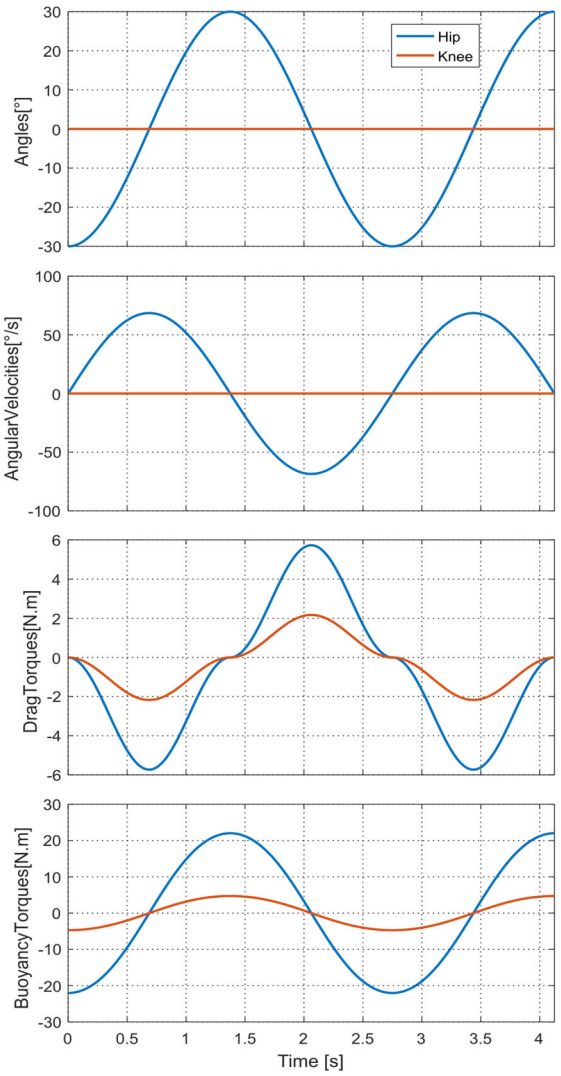

Figure 13. Buoyancy and drag torque outputs of the fluid model obtained during the single lower extremity computer simulations for hip extension exercise

Figure 13 also shows that buoyancy torques were found to be comparably larger in magnitude than drag torques. Drag torque values range from -6 N.m to +6 N.m and from -2 N.m to +2 N.m for hip and knee, respectively. On the other hand, buoyancy torques changes between -20 N.m and +20 N.m for hip and they change between -5 N.m and +5 N.m for knee. For this simulation, the fluid model yielded expected results. Moreover, the angle pattern used in the simulation and the torque outputs of the simulation were found to be highly comparable with the results of the healthy subject hip extension experiments presented in Chapter 5.

3.3. Support and Swing Transition Algorithm Simulations

The proposed support and swing transition algorithm was tested with computer simulations using the gait pattern data (including hip and knee angles) of a healthy subject.

Healthy subject gait pattern was collected during land walking with a high speed motion capture system. Mean of multiple gait cycles was used as the final reference gait pattern data.

The gait pattern data along with the lower extremity limb lengths of the subject was used to simulate the walk and to create a simple real time animation of it on the computer screen. The heel positions are fed to the stance and swing transition algorithm in the simulation and the calculated weighting variables on both lower extremities were displayed on the animation in real time as it was shown in Figure 14.

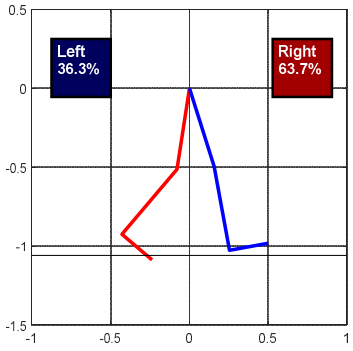

Figure 14. A picture of the created real time animation based on computer simulations

Additionally, the calculated weighting variable values on both lower extremities throughout the simulation are given in Figure 15. Note that the simulation was performed for 2 full gait cycles with a walking speed of 2.5 km/h.

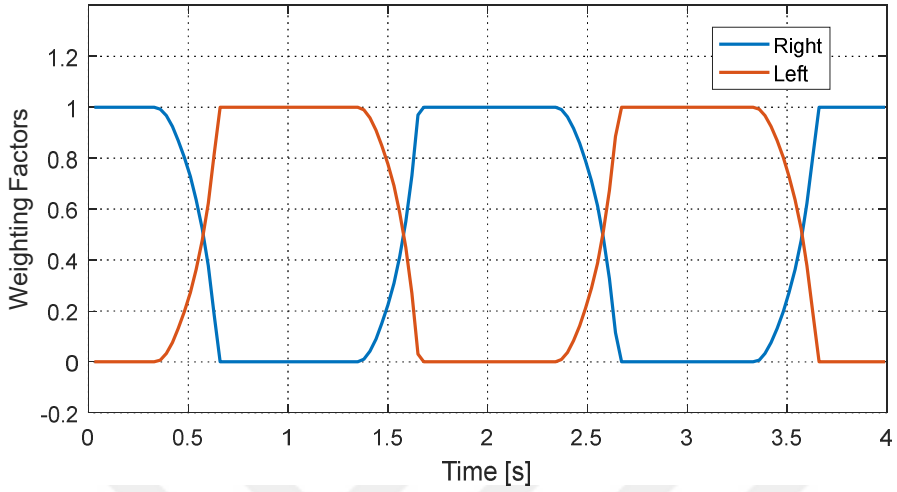

Figure 15. Weighting factors, α_R and α_L, calculated for right and left lower extremities, respectively, during the full gait computer simulations

The real time animation created and the weights plot indicate that the proposed stance and swing transition algorithm is highly effective at providing a smooth and definitive phase transition. The animation shows that heel strike and toe-off events, which are the start and the end of the transition region respectively, were caught precisely. As it can be seen in Figure 15, transitions occur smoothly and the algorithm works as it was designed. Figure 15 shows that a fast transition towards the end of the double stance phase is achieved as desired. Figure 15 also indicates that stance and swing phases are found to be roughly 60% and 40% of the gait cycle, respectively. These percentages are in agreement with the support and swing percentages found in literature [30], [80]. In addition, the transition region in Figure 15 roughly corresponds to 25% of the gait cycle and this value is also in agreement with the literature [81].

3.4. Full Gait Simulations

Torque outputs of the developed fluid model during full gait were determined with computer simulations again using the healthy subject gait pattern data obtained similarly to the data used for the support and swing transition algorithm simulations.

Before the simulations, dimensions for body segments of the healthy subject were inputted to the fluid model. For this simulation, fluid properties are selected so that they represent water's. Fluid properties are taken as $\rho_f = 998.6 kg/m^3$, $C_{D,C} = 0.4$ and $h_f = 1.3 m$ [14]. Also, flow velocity is kept zero, $\vec{v}_{flow} = 0 km/h$, during this simulation. Walking speed used during the simulation was 0.8 km/h. The reference gait pattern was applied to human body in the simulation and limb kinematics were determined. Based on the limb kinematics, torque outputs of the fluid model were calculated. The torque results obtained from the simulation are given in Figure 16. Note that stance phase in Figure 16 approximately corresponds to the region between 0 and 3.75 seconds.

Figure 16 shows that buoyancy torques were considerably larger in magnitude than drag ones. Drag torque values range from -2 N.m to +1 N.m and from -3 N.m to 0 N.m for hip and knee, respectively. On the other hand, buoyancy torques changes between -20 N.m and +20 N.m for hip and they change between -60 N.m and +60 N.m for knee. Note that buoyancy effects work directly against the weight of body segments and, consequently, assist the subject. Higher drag torques were observed during stance phase compared to swing phase at knee joint, as it can be seen in Figure 16. The reason for that is during the stance phase the whole body is propelled forward in the fluid and, therefore, drag effects resist this movement at the knee joint of the supporting lower extremity.

It should be noted that the gait data used in the simulation is obtained on land walking conditions. Gait patterns in actual fluid environment can slightly differ from the gait data used and the differences may cause deviations in the simulations.

The fluid model and the gait phase transition algorithm yielded expected results for the full gait simulation. Moreover, the torque outputs of the simulation were found to be highly comparable with the results of the healthy subject full gait experiments presented in Chapter 5.

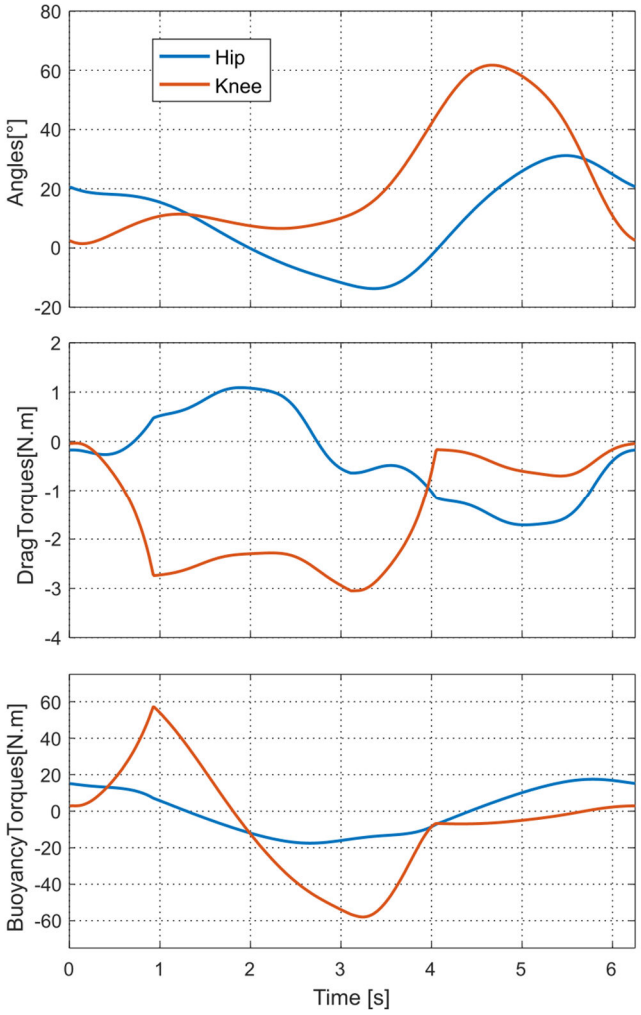

Figure 16. Joint angles, and buoyancy and drag torque outputs of the fluid model for the full gait computer simulations

3.5. Summary

This chapter covers the simulations performed based on the developed virtual fluid model, and the proposed support and swing phase detection algorithm. Buoyancy and drag models were verified by comparing the simulation outputs with previous

experimental studies in the literature. The support and swing transition algorithm was tested with full gait data and its outputs demonstrated a smooth transition between phases. Additionally, the fluid model torque outputs obtained in the simulations for single lower extremity exercises and full gait were evaluated.

In the following chapter, implementation of the developed fluid model and the proposed support and swing transition algorithm on a robotic gait trainer is presented. A control scheme based on the fluid model and the gait phase algorithm was created. A compensation model to counterbalance the weight and friction effects of the robotic parts was also developed and implemented.

CHAPTER 4

IMPLIMENTATION TO ROBOTIC GAIT TRAINER

This chapter includes the implementation of the fluid model and the gait phase transition algorithm on the robotic gait trainer. A separate model for compensating the weight and friction effects created by the robotic links was developed for the robotic implementation. The compensation model is explained and effectiveness of the compensation model is shown with experiments in the chapter.

4.1. RoboGait: The Robotic Gait Trainer Used

The algorithms and models developed in this study are implemented on a commercially available robotic body weight supported treadmill therapy device called RoboGait (BAMA Technology, Turkey) shown in Figure 17. RoboGait provides physical rehabilitation for patients with SCI, stroke, orthopedic and neurological disorders. It consists of a body weight support system, a visual motivation system, a treadmill and a robotic orthosis for lower extremity as shown in Figure 17.

Body weight support and orthosis are used to create weight off-loading effect of buoyancy forces and mimicking buoyancy and drag torques on the subject's legs, respectively. The robotic orthosis system can apply torques up to 270 Nm at the joints with linear actuators connected to four-bar linkages. Thus, the orthosis system is capable of supplying or resisting more than the amount of torque that an average

human lower extremity can produce [82]. Weight off-loading system can be adjusted from 0 to 140 kg. Treadmill speed in RoboGait can go up to 5 km/h.

RoboGait's visual motivation system is connected to the main computer, and it is capable providing avatar based audiovisual tasks to the subject. Movements of avatar are fully synchronized with the subject connected to the robotic system. Note that the visual motivation system was not utilized in the scope of this study.

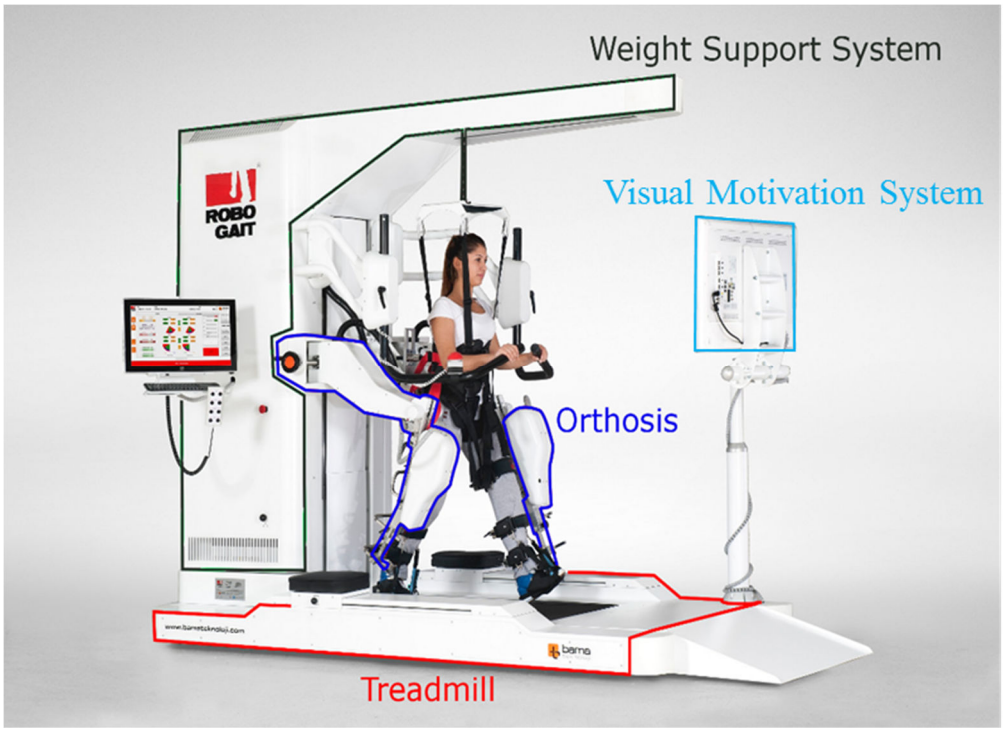

Figure 17. Picture of RoboGait with its labeled subsystems

4.2. Weight and Friction Compensation Model for Robotic Orthosis System

In order to apply the output torques from the fluid model, namely the buoyancy and drag torques, directly to the patient, orthosis mechanism should be transparent to the patient. This is achieved by counter balancing for the weight of whole mechanism and compensating for the weight and friction torques caused by links of the orthosis and the linear actuators. Torques created by weight and friction compensation model are calculated and added to the fluid model torques as shown in the Eqn. 4.1.

$$\vec{\tau}_{tot,(i-1),i} = \vec{\tau}_{f,(i-1),i} + \vec{\tau}_{weight,i} + \vec{\tau}_{fric,i} \tag{4.1}$$

Friction forces from the linear actuators and orthosis creates a non-consistent feeling during movement. Friction also creates an undesired resistance to the motion, making it especially hard to start the movement. Friction compensation model works for both dynamic and static cases. Dynamic friction compensation helps the patient in the direction of movement. Static friction compensation lowers the resistance when the patient wants to initiate a movement. Load cells, as shown in Figure 18, are utilized to assess the desired direction of motion when the system is below a certain velocity. Patient is supported in this direction as much as the static friction force which is obtained through a calibration method. If the angular velocity is above the threshold value, then the friction compensation force is taken to be in the same direction as the velocity vector. Main source of friction in the orthosis system is linear actuators due to their worm gear arrangement. Datasheets of the linear motors were utilized to estimate their friction characteristics. Other frictions such as mechanical bearing friction and etc. were observed to be insignificant compared to linear actuator friction and, therefore, they are neglected.

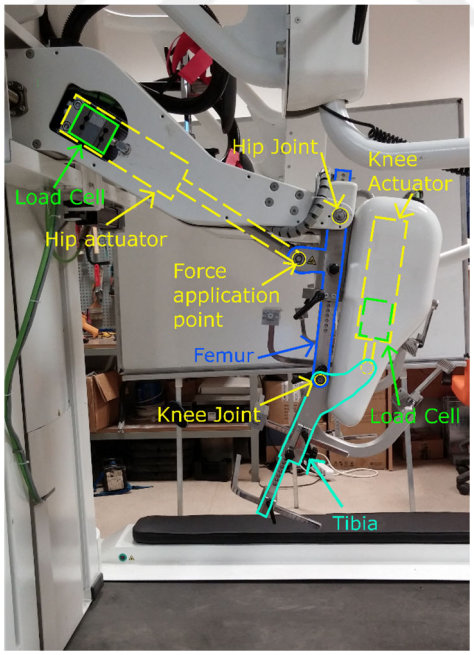

Figure 18. Actuator, load cell and mechanical link arrangements for RoboGait's orthosis system

Weight of the orthosis is also significantly high and can act high loads to the subject's legs if it is not compensated for. Various parts of the orthosis are weighed and the mass center of each piece is located. Then, these are reduced two point masses, one for the part between hip and knee joint, femur link, one for below the knee joint, tibia link. Moment created by the weight of these two point masses are calculated and counter balancing torques are included into the supplied torques by the actuators as explained in Eqn 4.1.

4.3. Overall Control Scheme

Control scheme used for the overall system can be seen in Figure 19. Gait velocity, $\vec{v}_{body}$, and flow velocity, $\vec{v}_{flow}$, can be set by the operator anytime during a session. The chosen walking speed determines the speed of the treadmill. Patient is assumed to be moving inside the fluid environment with the chosen speed along y-axis of the coordinate frame depicted in Figure 7. The selected flow speed is also taken to be along the y-axis. Parameters such as drag coefficient, water level and fluid density can also be altered which provides the flexibility to tailor the fluid environment for different patients and their conditions. An important thing to note is that the control system does not take any angle reference input as shown in Figure 19 since the goal is not to impose a path for the patient to follow, but rather creating a virtual field of static and dynamic forces determined by governing fluid mechanics principles, in which patient is moving.

Calculated buoyancy force acting on the whole body was set as the counter weight value for the body weight support system. The body weight support system is capable of exerting the same force amount within a certain vertical displacement allowing natural up-and-down movement of the subject's body during gait with the help of a special cam mechanism. Note that only fluid parameters that can change total buoyancy force to be applied by body weight support system are fluid level, h_f, and density of fluid, ρ_f.

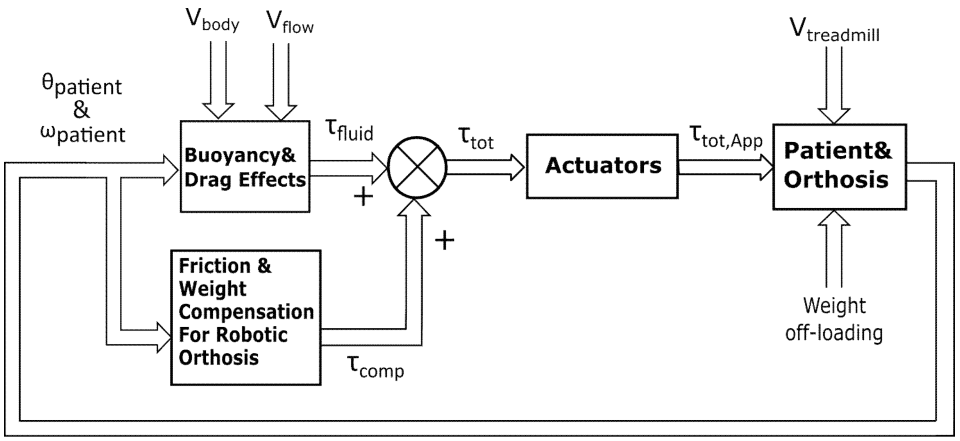

Figure 19. Diagram of control scheme used for the overall system

Torques acting on hip and knee joints due to fluid environment are calculated using the buoyancy and drag models. Then, fluid model torques are combined with the outputs of the weight and friction compensation model. These calculations are performed under the main control loop which operates at 20 Hz. Using the relations between joint torques and actuator forces determined by the four-bar mechanisms of the orthosis system, joint torque values are converted to target force values for linear actuators. Reaching these reference force targets is ensured by a closed loop PID controller which utilizes motor drivers consisting of FPGAs and power electronics. The bandwidth for this force control loop is 2.5 kHz.

Treadmill speed is also controlled by a PID controller. Walking speed set by the operator is the reference input for this feedback loop and an encoder is used for measuring the actual speed.

4.4. Experiments to Verify the Gravity and Friction Compensation Model

Effectiveness of the compensation model for friction and weight of the orthosis is verified by measuring applied torques from the orthosis. Verification is presented for hip joint only, since all joints shows the same characteristics. Orthosis system for hip is moved externally and data from the load cells attached to the orthosis are collected. Load cell and actuator arrangement for hip joint is shown in Figure 20. Torque due to

fluid effects that is expected to be applied to patient and the actual torque applied by the robotic orthosis are compared.

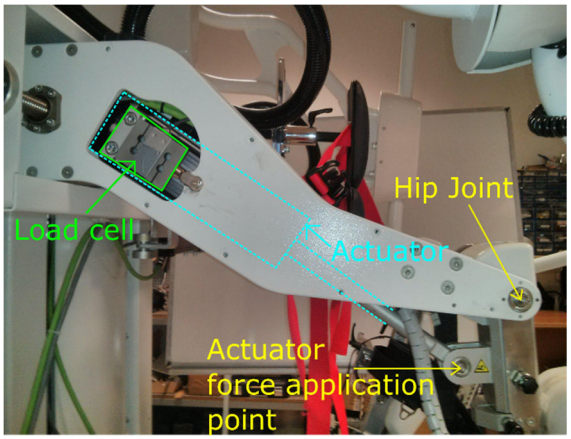

Figure 20. Load cell and actuator arrangement for hip joint

Force output was measured using the load cell attached to the linear actuator. The load cell readings were filtered via a low-pass and a moving average filters. Gravitational and inertial effects on orthosis were subtracted from these filtered measurements so that force applied to the subject can be reached. Then, these measurements were transformed into torque outputs using the calculated moment arm distances. The measured torque and the fluid model output torque for this experiment were presented in Figure 21.

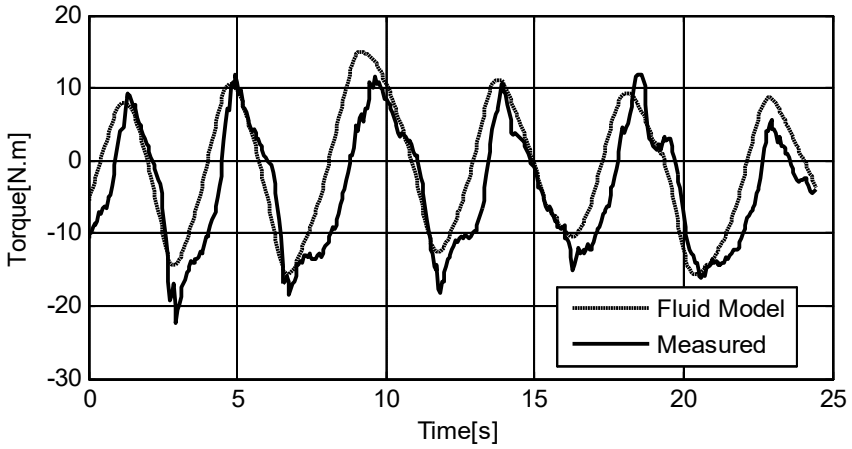

Figure 21. Torques expected due to fluid model and actual measured torques

As can be seen from Figure 21, fluid model output torques and measured joint torque values are highly comparable. The differences that appear might be caused by lateral forces acting on the load cells.

4.5. Summary

This chapter covers the implementation of the developed virtual fluid model and the proposed gait phase detection algorithm on the robotic gait trainer. Capabilities of the robotic gait trainer, RoboGait, was introduced and explained. Another model was developed to cancel out the friction and weight effects of robotic parts and to make the robotic system transparent to the subjects. The overall control scheme used on the robotic gait trainer was explained in detail. A special emphasis was made about how the control system works without needing a reference input. Lastly, the weight and friction compensation model was verified by experiments performed with load cells attached to the robotic system.

In the following chapter, the proposed method was tested with healthy subject experiments using the robotic gait trainer. Different experiment sets were carried out to evaluate the performance of the virtual fluid model implemented on the robotic gait trainer and the effects of varying fluid parameters.

CHAPTER 5

EXPERIMENTS WITH HEALTHY SUBJECTS

In this chapter, capability of the robotic gait trainer in realizing the fluid environment using the proposed method, effectiveness of the stance and swing transition algorithm, and effects of varying the fluid model parameters are explored through the experiments with healthy subjects using the robotic gait trainer, RoboGait.

Principles outlined in the Helsinki Declaration of 1975, as revised in 2000, were followed during all experimental procedures involving the human subjects. In addition, all experimental procedures used in this study were approved by the Institutional Ethical Review Board of Middle East Technical University.

All experimental data was collected with RoboGait's main computer at every 50 milliseconds except for high speed video recordings. A stand-alone video recorder was used for high speed visual data capture.

5.1. Single Lower Extremity Experiments

Characteristic of the robotic system depends highly on the parameters related to fluid model. Therefore, rehabilitation effects changes according to these parameters. To be able to tune rehabilitation effects, four parameters of the virtual fluid environment are selected as adjustable parameters which are $C_{D,C}$, ρ_f, $\vec{v}_{flow}$ and h_f. Depending upon needs of the patient, these parameters can be changed to adjust the buoyancy and drag

effects. Since these are also physical parameters, it is easier to visualize their effects on the patient for therapists.

Effects of adjustable fluid parameters were analyzed using a lower extremity exercise which is hip extension performed by single young healthy male subject. Age, body mass and body height of the subject were 25 years, 72 kg and 1.79 m, respectively. During this exercise the leg stays in swing phase. Since the aim of this experiment was to simulate a lower extremity exercises, upper body of the patient is assumed to be upright and stationary. Fluid level, h_f , is selected at the level of subject's Xiphoid process. Since upper body is taken as stationary for this particular experiment, this parameter does not affect the swinging leg. It only changes total buoyancy force which is to be applied by body weight support system. Thus, fluid level parameter was not varied in the experiment. Remaining parameters are changed and the subject is asked to perform the same movements with the same pace he could.

Angular position and velocity as well as the torques applied by the orthosis due to drag and buoyancy effects are collected for hip extension exercise and results are given in Figure 22. The subject was able to follow the same pattern but with varying effort. Results show that increasing drag coefficient amplifies drag torques whereas increasing fluid density increases the magnitude of buoyancy and drag torques together. Flow velocity increases drag force significantly in the flow direction which is apparent in increased drag torques. Since similar angular patterns are followed, buoyancy torques came out to be similar for all cases except that fluid density parameter was changed.

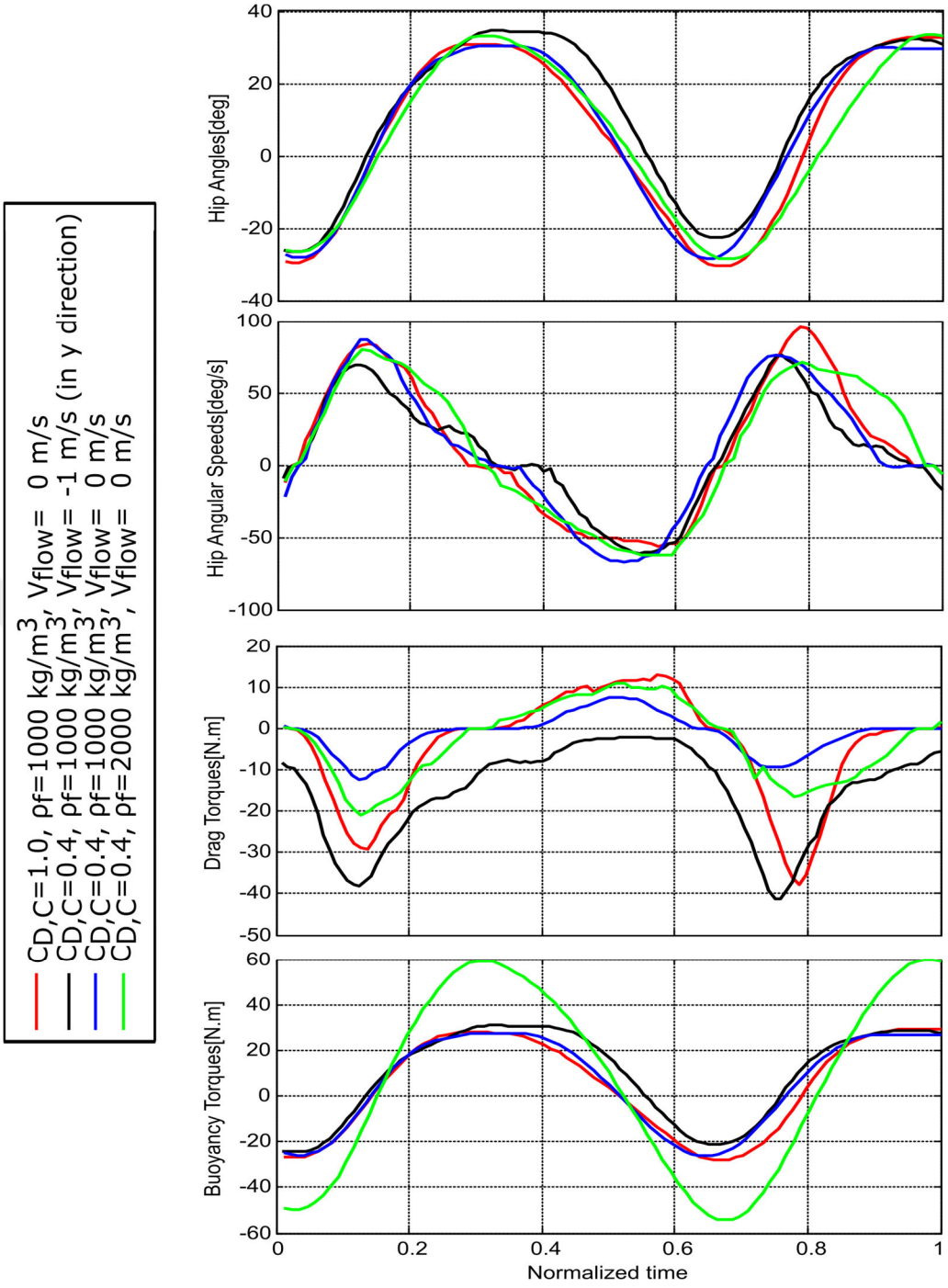

Figure 22. Effects of adjustable parameters on buoyancy and drag torque outputs of the model for hip extension exercise with single lower extremity

5.2. Experiments for Complete Gait

Full gait experiments were done with 6 healthy male adult subjects using RoboGait. Mean ± SD age, body mass and body height of the subjects were 25.7±0.5 years, 70.7±7.9 kg and 1.78±0.03 m, respectively.

The stance and swing phase transition algorithm should be able to detect phase changes in real time without significant deviations in order for the fluid model to work properly during full gait. Therefore, the developed algorithm needed to be tested with different subjects for a considerable number of gait cycles so that its performance can be verified. A set of experiments were designed and performed to verify the proposed stance and swing phase detection algorithm, and the results are presented in this section.

Another important point was to determine the effects of applying the fluid model forces and torques in the robotic gait trainer on gait characteristics of subjects compared to not applying them. For that purpose, experiments were designed and implemented for healthy subjects to walk in land and water conditions using the robotic gait trainer. The fluid model forces and torques were not applied in land conditions whereas they were included in water conditions. The weight and friction compensation model was implemented in both conditions since the transparency of the robotic system's mechanical effects to subjects was required in both. Water was selected as the fluid in these experiments since gait characteristics for water environment are well reported in the literature. Hence, the legitimacy of the fluid model can be assessed by comparing the outcomes of the experiments with the gait characteristics found in the literature for an actual fluid environment. The results obtained in these experiments are also presented in this section.

Lastly, experiments were done to observe the effects of changing the fluid model parameters. These sets of experiments were conducted in order to create a guideline for future therapy sessions with the proposed method. The experiment sets aim to map the changes in torque and gait characteristics into the guideline for each individual fluid model parameter varied. Thus, the therapist will be able to determine the set of fluid model parameters that are most suitable for a specific patient based on the

guideline. Fluid density, drag coefficient and fluid level were varied in one of the experiment sets. In the other set, different flow velocities were applied on the subjects. The results of these experiments are also given in this section of the thesis.

The overall experimental flow used for complete gait experiments is provided at Appendix B. Figure 23 below shows one of the subjects walking with the robotic gait trainer during an experiment session for complete gait.

Figure 23. A picture taken during one of the experiment sessions with the healthy subjects

All experimental data collected within one experiment session for a single subject is divided into gait cycles. Since the number of data points in each cycle can be different, the time of data points in each cycle are normalized between 0.0 and 1.0 with 0.001 increments. Then, the cycle divided and time normalized data of all subjects for the

same experimental sessions are combined. Means and standard deviations are calculated for each increment point on the normalized time axis.

5.2.1. Stance and Swing Transition Algorithm Experiments

Performance of the stance swing phase detection algorithm was tested when the healthy subjects were walking with RoboGait in land conditions. This experiment was done in land conditions rather than fluid environment so that the results of the proposed algorithm can be compared to gait studies for land walking in literature. The subjects' gait during this experiment was recorded with high speed video camera to analyze actual stance-swing transition in order to compare with the outputs of the algorithm.

The walking speed was set to +0.8 km/h and the stance and swing phase transition algorithm outputs were collected while the healthy subjects were walking in land walking conditions. For land walking with RoboGait, only weight and friction compensation torques are applied to the subject and fluid model torques are excluded. Also, body weight support of RoboGait is not used for land conditions. Actual stance-swing transitions for the subjects' gait were determined from 120 fps video recordings of the experiment sessions. Percentage time spent for actual stance is found out to be 62.47±3.77%. The proposed stance swing phase detection algorithm predicted support phase as 61.55±5.53%. These are the mean values and standard deviations for gait cycles (N=250) of all subjects during these experiment sessions. Mean values of the predicted and actual support percentages were found to be in the close vicinity of each other. Both the outputs of the algorithm and the video measurements found to be comparable with the values for land walking in the literature [9]. Outputs of the stance and swing algorithm, and high speed video recordings are presented in time domain on Figure 24. In the figure, vertical dashed lines indicate the start and end of phase transitions obtained from high speed video recording, and gait phases (Stance, Swing or "DS"-Double Support) at the regions divided by the vertical lines are indicated. Figure 24 shows that the support and swing transition algorithm ensures clear and smooth transition between phases. It can also be seen that start and finish instants of the transition regions of both video and algorithm outputs are found to be highly concurrent. Transition phase corresponds to double-limb support in which body weight

is gradually transferred from one lower extremity to the other. Total transition percentage predicted by the algorithm is comparable with 25% total double-limb support value for one gait cycle found in the literature [81].

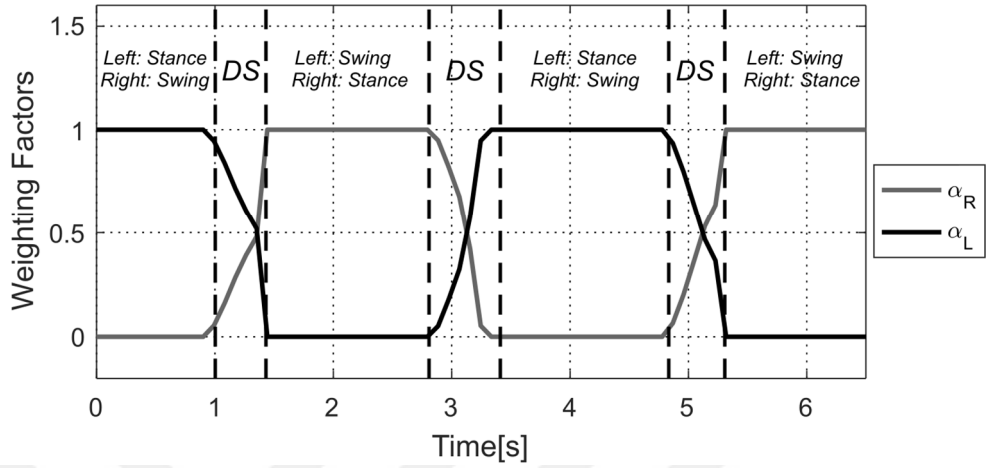

Figure 24. Outputs of the support and swing transition algorithm for +0.8 km/h walking speed of healthy subjects in land walking conditions with RoboGait

5.2.2. Land vs Water Experiments

In order to compare gait kinematics of healthy adults for land and fluid walking with RoboGait, the subjects were instructed to walk with a pace which they feel comfortable for each case. Literature contains abundant previous studies for land and water gait comparison. In order to make the outputs of the experiment with RoboGait comparable with previous studies in literature, values of fluid parameters in the model were set such that they are the same with water's. Thus, the gait characteristics obtained with the robotic gait trainer can be compared with the gait characteristics obtained in previous experimental studies for real water and land environments. Capability of the robotic gait trainer with the proposed method to realize virtual fluid environment was assessed by making this comparison.

During the experiments for comparing land and water walking, land walking condition is applied as explained in the gait phase detection experiments section. For water walking, fluid parameters are selected so that it represents water. Fluid level is set to

be $h_f = 1.3m$ and circular drag coefficient is chosen as $C_{D,C} = 0.4$ [14]. Density of water is taken as $\rho_f = 998.6\,kg/m^3$ and flow velocity is set to zero, $\vec{v}_{flow} = 0km/h$. Total buoyancy forces on the subjects' body are calculated and set at the body weight support system in water walking case, which roughly corresponds to 68% of each subjects' body weight. Walking speeds for both cases are selected so that they are just below the subjects' comfort level and they are set as the treadmill speed.

Joint angles and angular velocities for walking with land and water conditions are given in Figure 25. Note that stance and swing phases correspond roughly to 0-60% and 60-100% of gait cycle in the figure, respectively. It can be seen from Figure 25 that range of motions (ROM) for hip and knee are decreased for water walking which is consistent with the findings in literature [12]. The difference in peak hip and knee extension angles between land and water becomes as high as 10° for both joints.

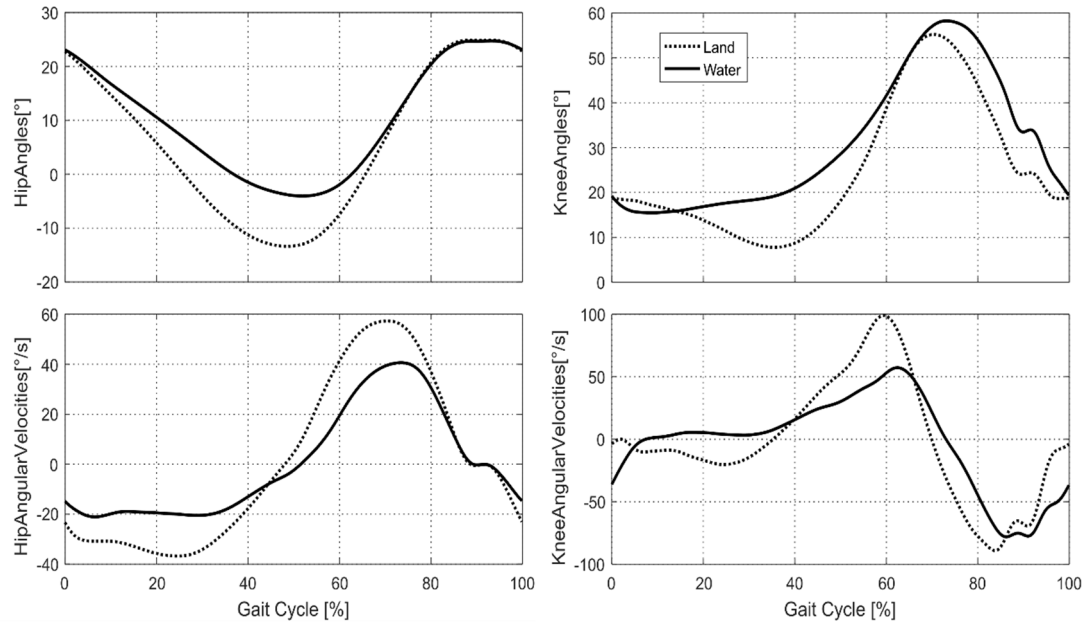

Figure 25. Mean hip and knee angles and angular velocities of the healthy subjects' gait cycles (N=850) for land and water walking conditions with RoboGait

Figure 25 also shows that angular velocities are attenuated for water walking. This can be explained by viscous characteristics of the fluid environment which results in higher dampening effects. This is found to be comparable with the previous experimental

study in the literature [8]. Knee angle patterns for land and water conditions found to be similar with [83], including a late knee flexion peak and the lack of knee loading response for water walking case.

For Figure 25, averages of standard deviations associated with all subjects' gait data are calculated as: ±4.30˚ in land and ±4.40˚ in water for hip angles, ±7.80˚ in land and ±7.39˚ in water for knee angles, ±7.98˚/s in land and ±6.48˚/s in water for hip angular velocities, and ±24.59˚/s in land and ±17.36˚/s in water for knee angular velocities.

Table 2 contains information on spatial and temporal gait parameters of land and water walking comparison experiment. It can be seen that significant changes in stride duration and gait speed are observed whereas stride length and support phase percentage remains mostly unchanged. These outcomes are in agreement with the results of [83].

Table 2. Means (±SD) of temporal and spatial gait parameters of the healthy subjects' gait cycles (N=850) for land and water walking conditions with RoboGait

	Land	Water
Stride Duration (s)	2.66±0.35	3.17±0.46
Gait Speed* (km/h)	+1.58±0.10	+1.34±0.10
Stride Length (m)	1.17±0.10	1.18±0.13
Support Phase (%)	55.6±7.3	54.8±6.3

5.2.3. Experiments with Varied Drag Coefficient, Fluid Density and Fluid Level

To show the effects of changing fluid parameters on gait kinematics and fluid model joint torques, another experiment was conducted. Fluid parameters of water were used as baseline and during the experiment drag coefficient, fluid density and fluid level were varied while the healthy subjects were performing gait with RoboGait.

Four different fluid parameter sets were applied to each subject during the experiments. Fluid properties of Base Case are selected as $\rho_f = 998.6\,kg/m^3$, $C_{D,C} = 0.4$ and $h_f = 1.3\,m$. Only one parameter is changed in each parameter set with

respect to Base Case. The exact values of drag coefficient, fluid density and fluid level utilized in each parameter set are given in the legend of Figure 26. Walking speed is set to +1.0 km/h and flow velocity is set to zero, $\vec{v}_{flow} = 0 km/h$, for all four cases. Total buoyancy forces on the subjects' body are calculated and set at the body weight support system, which roughly corresponds to 80%, 68% and 43% of each subjects' body weight for High Fluid Density Case, Base Case and High Drag Coefficient Case, and Low Fluid Level Case, respectively.

Effects of varying the fluid parameters on joint angles, drag torques and buoyancy torques can be seen from Figure 26. The data was collected at the walking speed of +1.0 km/h for all four cases in the experiment sessions. For the figure, torques are normalized using body weight (BW) and leg length (LL) of each subject and given as percentages. Also, note that stance and swing phases correspond roughly to 0-60% and 60-100% of gait cycle in the figure, respectively.

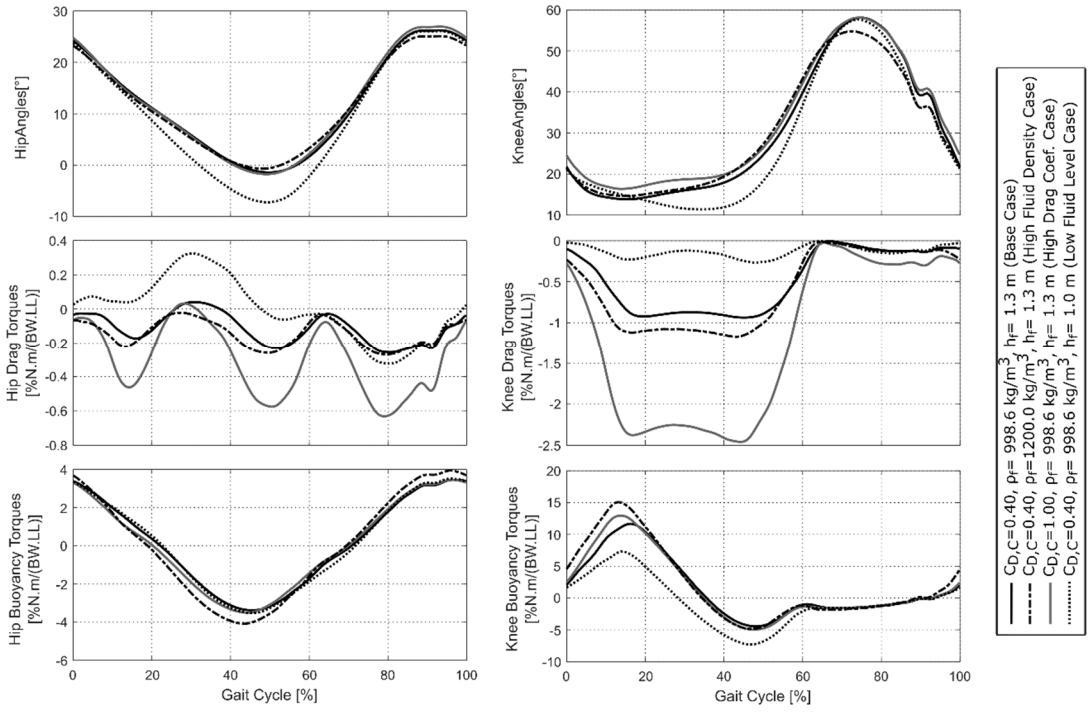

Figure 26. Mean values of angles, and applied drag and buoyancy torques for hip and knee joints during the healthy subjects' gait cycles (N=700) with four different fluid model parameter sets (refer to the legend of figure) on RoboGait

Figure 26 shows that buoyancy torques which create counter balancing effects for the weights of body segments are higher in magnitude compared to drag torques. As it can be seen in Figure 26, increasing the fluid density resulted in amplified drag and buoyancy torques in both knee and hip joints with respect to Base Case. Hip and knee angle patterns did not change significantly compared to Base Case except for a slight decrease in peak knee flexion angle in High Fluid Density Case. Unlike fluid density, increasing drag coefficient only amplifies drag torques which can be seen from Figure 26. For High Drag Coefficient Case, angular patterns remained the same. For Low Fluid Level Case, upper body effects are diminished since upper body is less immersed in the virtual fluid environment with respect to Base Case. The figure shows that peak extension angles and ROMs are increased for hip and knee joints in Low Fluid Level Case. The knee loading response, higher ROMs and higher hip extension imply that gait characteristics of Lower Fluid Level Case becomes closer to the gait characteristics of land walking conditions from Figure 25. This is expected since decreasing fluid level further would eventually converge into land walking conditions by diminishing fluid effects. In Low Fluid Level Case, hip and knee drag torques during the stance phase are shifted in positive direction due to the decrease in upper body drag forces which counter balance drag forces on the lower extremities. Hip buoyancy torque is not significantly affected. However, reduced upper body buoyancy force due to lower fluid level resulted in decreased buoyancy torque in the knee joint which, consequently, decreases the assistive effect.

For Figure 26, averages of standard deviations associated with all subjects' gait data are calculated as: ±3.78˚ for hip angles, ±8.54˚ for knee angles, ±0.138 %N.m/(BW.LL) for hip drag torques, ±0.252 %N.m/(BW.LL) for knee drag torques, ±0.671 %N.m/(BW.LL) for hip buoyancy torques and ±3.106 %N.m/(BW.LL) for knee buoyancy torques.

As it can be seen in Table 3, mean spatial and temporal gait parameters remains within the margin of error for the varied fluid model parameters. This indicates that mean temporal and spatial gait parameters are preserved although there are some changes in the angular gait patterns as stated.

Table 3. Means (±SD) of temporal and spatial gait parameters of the healthy subjects' gait cycles (N=700) for four different fluid model parameter sets with RoboGait. Only one parameter is changed in each parameter set with respect to Base Case (refer to the table).

	Base Case	$\rho_f = 1200 kg/m^3$	$C_{D,C} = 1.0$	$h_f = 1.0 m$
Stride Duration (s)	3.59±0.38	3.61±0.43	3.54±0.38	3.58±0.47
Stride Length (m)	1.00±0.10	1.00±0.12	0.98±0.10	0.99±0.13
Support Phase (%)	58.1±4.6	59.4±5.8	58.2±5.8	59.9±4.1

5.2.4. Flow Experiments

Flow velocity is found to be another parameter that can be used to characterize the therapy. The last experiment in the scope of this study was performed to show flow effects on gait. In this experiment, different flow velocities for the fluid model were applied as the healthy subjects performed gait with RoboGait.

Three different flow velocities, which are $\vec{v}_{flow} = 0\,km/h$, $\vec{v}_{flow} = +0.8\,km/h$ and $\vec{v}_{flow} = -0.8\,km/h$, were applied to each subject during the experiments. Walking speed is set to +1.0 km/h and fluid properties are adopted as $\rho_f = 998.6\,kg/m^3$, $C_{D,C} = 0.4$ and $h_f = 1.3\,m$ for all three flow velocity cases. Total buoyancy forces on the subjects' body are calculated and set at the body weight support system, which roughly corresponds to 68% of each subjects' body weight. Torques are normalized using body weight (BW) and leg length (LL) of each subject and given as percentages.

Figure 27 shows impacts of varying flow velocity on joint angles, angular velocities and drag torques. Note that stance and swing phases correspond roughly to 0-60% and 60-100% of gait cycle in the figure, respectively. As can be seen from the figure, hip and knee drag torques are the highest for the negative flow whereas they are the lowest for the positive flow. This is expected because as can be seen from Eqn. 2.6, drag torques acting on each joint highly depends on relative velocity of the body segment with respect to the fluid. The relative velocity is higher for the negative flow and lower for the positive flow. Even though drag torques vary, no significant changes occurred in hip angle pattern. However, knee angle patterns are effected. Knee is observed to be bending more during support phase of negative flow velocity case. This can be

explained by the increased resistance on the subjects' body due to the negative flow. Similarly, knee is slightly more extended at support phase for positive flow velocity since the resistance is lower in this case.

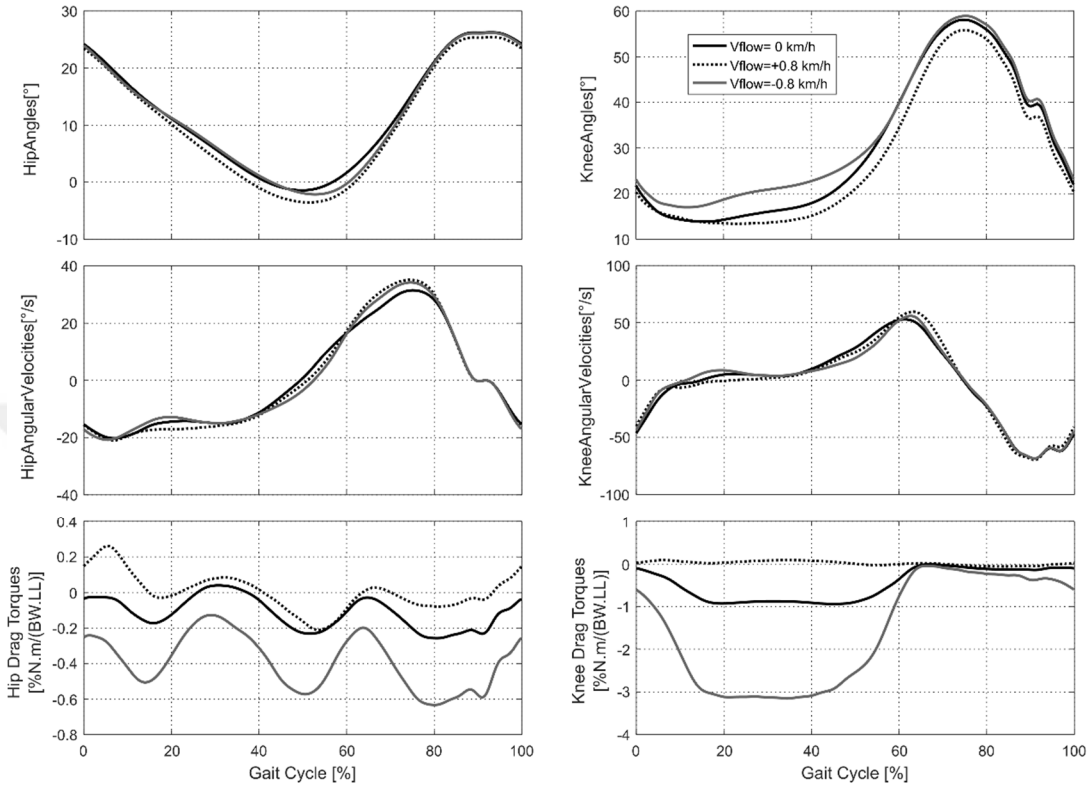

Figure 27. Mean values of angles, angular velocities and drag torques for hip and knee joints during the healthy subjects' gait cycles (N=700) with different flow velocities (refer to legend of the figure) on RoboGait

For Figure 27, averages of standard deviations associated with all subjects' gait data are calculated as: ±3.62˚ for hip angles, ±7.71˚ for knee angles, ±5.68˚/s for hip angular velocities, ±15.22˚/s for knee angular velocities, ±0.148 %N.m/(BW.LL) for hip drag torques and ±0.317 %N.m/(BW.LL) for knee drag torques.

Table 4 represents mean spatial and temporal gait parameters for the experiments done to determine effects of varying flow velocity. Aforementioned changes in gait pattern and drag torques for varied flow velocities do not cause any observable difference in stride durations, stride lengths or percentage of support phase. This is in agreement with the results of the experiment where fluid parameters are varied.

Table 4. Means (±SD) of temporal and spatial gait parameters of the healthy subjects' gait cycles (N=700) for different flow velocities (refer to the table) with RoboGait.

	$\vec{v}_{flow} = 0km/h$	$\vec{v}_{flow} = +0.8km/h$	$\vec{v}_{flow} = -0.8km/h$
Stride Duration (s)	3.59±0.38	3.51±0.36	3.57±0.34
Stride Length (m)	1.00±0.10	0.97±0.10	0.99±0.09
Support Phase (%)	58.1±4.6	59.1±4.5	57.7±5.6

5.3. Summary

This chapter covers the experiments done with healthy subjects for the testing of the proposed robotic physical therapy method. Single lower extremity and full gait exercises were performed in the conducted experiments. Experiment sets with different fluid conditions were carried out to evaluate the performance of the virtual fluid model implemented on the robotic gait trainer. Changes in the torque outputs of the fluid model and the movement characteristics of healthy subjects were evaluated using the experimental outcomes. Additionally, the support and swing transition algorithm was tested with multiple subjects in real time and its effectiveness was verified.

In the following chapter, conclusions driven from this study are presented along with potential future directions for the study.

CHAPTER 6

CONCLUSION & FUTURE WORK

6.1. Conclusion

In this thesis, human gait in a fluid was modeled and this model was used to recreate the same effects as a novel control strategy for robotic gait trainers in which no predefined path is required and the therapy parameters are fully adjustable.

Torques acting on human lower extremity in a fluid was modeled by approximating human body as 3D rigid bodies and buoyancy and drag torques were calculated accordingly. Accuracy of this model was checked by comparing its outputs from computer simulations with previous experimental studies. These comparisons showed that the model generates fairly close torque outputs.

A control algorithm was developed to control the torques exerted by the robotic orthosis. Experiments showed that torques from the virtual fluid environment was successfully transferred to the subject. Since the model makes it possible to adjust parameters like drag coefficient, fluid density and flow velocity, experiments were done to assess their effects on a common exercise such as hip extension. Results clearly demonstrate that the effects of each of these parameters altered the model output in the desired way.

For complete gait implementation on the robotic system, an algorithm was developed to detect if a lower extremity is at swing, stance and transition phase since joint torques acting on swing and stance phases are different. Experiments with healthy subjects showed that this algorithm was able to detect the swing and stance transition correctly. Note that usage of the developed phase detection algorithm is not limited to this study. It can also be implemented in other applications which requires a smooth transition between gait phases.

It was shown that aquatic therapy in gait rehabilitation can be realized by a robotic gait trainer. Experiments were performed to examine the effects of varying fluid density, drag coefficient, fluid level and flow velocity on gait characteristics of healthy subjects. Fluid model is proven to be able to produce the expected changes in torque outputs. Angle measurements from hip and knee joints indicated that the effects of these changes in torques are well reflected to the subjects. No significant changes were observed in mean temporal and spatial gait parameters while varying fluid parameters or flow velocity. Further alterations of these parameters and flow velocity might affect the mean temporal and spatial gait parameters, as well. For these experimental results, it should be noted that the difference between gait characteristics of the subjects is one of the major contributing factors of the standard deviations.

The proposed method was implemented on a robotic gait trainer with a robotic orthosis. However, the methodology discussed here could be used with different robots that interact with the lower extremity of human body.

In a lot of cases, patients with conditions such as SCI, cerebral palsy and stroke cannot recover to the point of walking in the “ideal” pattern, instead they just have a functional recovery [84]. The environment for natural experimentation provided by this novel proposed method is intended to promote functional recovery. The fittest gait pattern which minimizes the effort for a patient’s unique condition is expected to be naturally adopted by that patient. The results presented in this thesis can be used as a guideline for the suitable parameter selection during therapy sessions utilizing the proposed rehabilitation method.

6.2. Future Work

This research can be extended so that method of simulating gait therapy in fluid environment can become a feasible option for robotic gait trainers. Future plans on this research includes repeating the experiments with healthy subjects while collecting EMG data to verify muscle activity induced by this method. Effects of commonly used tools in underwater therapies like hydro boots and buoyancy cuffs can also be added to model. Clinical trials with patient groups will also be performed to assess the effectiveness of this method as a therapy.

Additionally, visual motivation system of RoboGait can be integrated in this study. Visual motivation system can be utilized to augment the virtual fluid environment experience by providing audiovisual feedback as well as to motivate patients through special audiovisual tasks designed for improving their rehabilitation progress.

This research is planned to be commercialized as a new therapy function for RoboGait, the robotic gait trainer used in the experiments.

REFERENCES

[1] B. C. Marsh, S. L. Astill, A. Utley, and R. M. Ichiyama, "Movement rehabilitation after spinal cord injuries: Emerging concepts and future directions," *Brain Res. Bull.*, vol. 84, no. 4–5, pp. 327–336, 2011.

[2] P. Musienko, J. Heutschi, L. Friedli, R. Van den Brand, and G. Courtine, "Multi-system neurorehabilitative strategies to restore motor functions following severe spinal cord injury," *Exp. Neurol.*, vol. 235, no. 1, pp. 100–109, 2012.

[3] K. Fouad and W. Tetzlaff, "Rehabilitative training and plasticity following spinal cord injury," *Exp. Neurol.*, vol. 235, no. 1, pp. 91–99, 2012.

[4] L. Ada, C. M. Dean, J. M. Hall, J. Bampton, and S. Crompton, "A treadmill and overground walking program improves walking in persons residing in the community after stroke: a placebo-controlled, randomized trial," *Arch. Phys. Med. Rehabil.*, vol. 84, no. 10, pp. 1486–1491, 2003.

[5] R. F. Macko *et al.*, "Treadmill exercise rehabilitation improves ambulatory function and cardiovascular fitness in patients with chronic stroke: A randomized, controlled trial," *Stroke*, vol. 36, no. 10, pp. 2206–2211, 2005.

[6] P. W. Duncan *et al.*, "Protocol for the Locomotor Experience Applied Post-stroke (LEAPS) trial: a randomized controlled trial," *BMC Neurol.*, vol. 7, no. 1, p. 39, 2007.

[7] "Department of Physical Therapy - College of Public Health and Health Professions - University of Florida." [Online]. Available: http://pt.phhp.ufl.edu/research/locomotor-training/. [Accessed: 22-May-2017].

[8] M. I. V. Orselli and M. Duarte, "Joint forces and torques when walking in shallow water.," *J. Biomech.*, vol. 44, no. 6, pp. 1170–5, 2011.

[9] D. Iucksch, V. Israel, D. Ribas, and E. Manffra, "Gait characteristics of persons with incomplete spinal cord injury in shallow water," *J. Rehabil. Med.*, vol. 45, no. 9, pp. 860–865, 2013.

[10] K. Kaneda, H. Wakabayashi, D. Sato, and T. Nomura, "Lower Extremity

Muscle Activity during Different Types and Speeds of Underwater Movement," *J. Physiol. Anthropol.*, vol. 26, no. 2, pp. 197–200, 2007.

[11] K. Masumoto and J. a Mercer, "Biomechanics of human locomotion in water: an electomyographic analysis.," *Exerc. Sport Sci. Rev.*, vol. 36, pp. 160–169, 2008.

[12] T. Miyoshi, T. Shirota, S. Yamamoto, K. Nakazawa, and M. Akai, "Effect of the walking speed to the lower limb joint angular displacements, joint moments and ground reaction forces during walking in water.," *Disabil. Rehabil.*, vol. 26, no. February 2016, pp. 724–732, 2004.

[13] T. Pöyhönen, H. Kyröläinen, K. L. Keskinen, A. Hautala, J. Savolainen, and E. Mälkiä, "Electromyographic and kinematic analysis of therapeutic knee exercises under water," *Clin. Biomech.*, vol. 16, no. 6, pp. 496–504, 2001.

[14] T. Poyhonen, K. L. Keskinen, a Hautala, E. Malkia, T. Pöyhönen, and E. Mälkiä, "Determination of hydrodynamic drag forces and drag coefficients on human leg/foot model during knee exercise.," *Clin. Biomech.*, vol. 15, no. 4, pp. 256–260, 2000.

[15] J. C. Colado and N. T. Triplett, "Monitoring the Intensity of Aquatic Resistance Exercises With Devices That Increase the Drag Force: An Update," *Strength Cond. J.*, vol. 31, no. 3, pp. 94–100, 2009.

[16] B. E. Becker, "Aquatic Therapy: Scientific Foundations and Clinical Rehabilitation Applications," *PM R*, vol. 1, no. 9, pp. 859–872, 2009.

[17] Z. Zhu *et al.*, "Hydrotherapy vs. conventional land-based exercise for improving walking and balance after stroke: A randomized controlled trial," *Clin. Rehabil.*, p. 0269215515593392-, 2015.

[18] H. S. Lim and S. Yoon, "The Influence of Short-term Aquatic Training on Obstacle Crossing in Gait by the Elderly," *J. Phys. Ther. Sci.*, vol. 26, no. 8, pp. 1219–1222, 2014.

[19] H. S. Lim, S. Y. Roh, and S. Yoon, "An 8-week Aquatic Exercise Program is Effective at Improving Gait Stability of the Elderly.," *J. Phys. Ther. Sci.*, vol. 25, no. 11, pp. 1467–70, 2013.

[20] D. K. Noh, J.-Y. Lim, H.-I. Shin, and N.-J. Paik, "The effect of aquatic therapy on postural balance and muscle strength in stroke survivors--a randomized controlled pilot trial.," *Clin. Rehabil.*, vol. 22, no. 10–11, pp. 966–76, 2008.

[21] T. Tsourlou, A. Benik, K. Dipla, A. Zafeiridis, and S. Kellis, "The Effects of a Twenty-Four–Week Aquatic Training Program on Muscular Strength Performance in Healthy Elderly Women," *J. Strength Cond. Res.*, vol. 20, no. 4, p. 811, 2006.

[22] T. Pöyhönen, S. Sipilä, K. L. Keskinen, A. Hautala, J. Savolainen, and E. Mälkiä, "Effects of aquatic resistance training on neuromuscular performance in healthy women.," *Med. Sci. Sports Exerc.*, vol. 34, no. 12, pp. 2103–9, 2002.

[23] "Physicians Physical Therapy Center." [Online]. Available: http://www.pptaquasports.com/aquatic-therapy.html. [Accessed: 22-May-2017].

[24] T. Jung, Y. Ozaki, B. Lai, and K. Vrongistinos, "Comparison of energy expenditure between aquatic and overground treadmill walking in people post-stroke," *Physiother. Res. Int.*, vol. 19, no. 1, pp. 55–64, 2014.

[25] D. Lee, S. Jeong, and Y. Kim, "Effects of underwater treadmill walking training on the peak torque of the knee in hemiplegic patients.," *J. Phys. Ther. Sci.*, vol. 27, no. 9, pp. 2871–3, 2015.

[26] S.-E. Park *et al.*, "Comparison of Underwater and Overground Treadmill Walking to Improve Gait Pattern and Muscle Strength after Stroke," *J. Phys. Ther. Sci.*, vol. 24, no. 11, pp. 1087–1090, 2012.

[27] S. L. Stevens, J. L. Caputo, D. K. Fuller, and D. W. Morgan, "Effects of underwater treadmill training on leg strength, balance, and walking performance in adults with incomplete spinal cord injury.," *J. Spinal Cord Med.*, vol. 38, no. 1, pp. 91–101, 2015.

[28] S. W. Park, K. J. Lee, D. C. Shin, S. H. Shin, M. M. Lee, and C. H. Song, "The effect of underwater gait training on balance ability of stroke patients.," *J. Phys. Ther. Sci.*, vol. 26, no. 6, pp. 899–903, 2014.

[29] N. P. Greene, B. S. Lambert, E. S. Greene, A. F. Carbuhn, J. S. Green, and S. F. Crouse, "Comparative efficacy of water and land treadmill training for overweight or obese adults," *Med. Sci. Sports Exerc.*, vol. 41, no. 9, pp. 1808–1815, 2009.

[30] T. Jung, D. Lee, C. Charalambous, and K. Vrongistinos, "The Influence of Applying Additional Weight to the Affected Leg on Gait Patterns During Aquatic Treadmill Walking in People Poststroke," *Arch. Phys. Med. Rehabil.*, vol. 91, no. 1, pp. 129–136, Jan. 2010.

[31] "HydroWorx." [Online]. Available: https://www.hydroworx.com/. [Accessed: 23-May-2017].

[32] L. Marchal-Crespo and D. J. Reinkensmeyer, "Review of control strategies for robotic movement training after neurologic injury," *J. Neuroeng. Rehabil.*, vol. 6, no. 1, p. 20, 2009.

[33] T. Nef, M. Mihelj, and R. Riener, "ARMin: a robot for patient-cooperative arm therapy," *Med. Biol. Eng. Comput.*, vol. 45, no. 9, pp. 887–900, Sep. 2007.

[34] S. Kousidou, N. G. Tsagarakis, C. Smith, and D. G. Caldwell, “Task-Orientated Biofeedback System for the Rehabilitation of the Upper Limb,” in *2007 IEEE 10th International Conference on Rehabilitation Robotics*, 2007, pp. 376–384.

[35] A. Montagner *et al.*, “A pilot clinical study on robotic assisted rehabilitation in VR with an arm exoskeleton device,” in *2007 Virtual Rehabilitation*, 2007, pp. 57–64.

[36] L.-Q. Zhang, H.-S. Park, and Y. Ren, “Developing an Intelligent Robotic Arm for Stroke Rehabilitation,” in *2007 IEEE 10th International Conference on Rehabilitation Robotics*, 2007, pp. 984–993.

[37] R. C. V. Loureiro and W. S. Harwin, “Reach & Grasp Therapy: Design and Control of a 9-DOF Robotic Neuro-rehabilitation System,” in *2007 IEEE 10th International Conference on Rehabilitation Robotics*, 2007, pp. 757–763.

[38] H. I. Krebs *et al.*, “Robot-Aided Neurorehabilitation: A Robot for Wrist Rehabilitation,” *IEEE Trans. Neural Syst. Rehabil. Eng.*, vol. 15, no. 3, pp. 327–335, Sep. 2007.

[39] S. Guo, W. Zhang, J. Guo, J. Gao, and Y. Hu, “Design and kinematic simulation of a novel exoskeleton rehabilitation hand robot,” in *2016 IEEE International Conference on Mechatronics and Automation*, 2016, pp. 1125–1130.

[40] C. Wang *et al.*, “Development of a rehabilitation robot for hand and wrist rehabilitation training,” in *2015 IEEE International Conference on Information and Automation*, 2015, pp. 106–111.

[41] G. Kwakkel, R. C. Wagenaar, T. W. Koelman, G. J. Lankhorst, and J. C. Koetsier, “Effects of Intensity of Rehabilitation After Stroke : A Research Synthesis,” *Stroke*, vol. 28, no. 8, pp. 1550–1556, 1997.

[42] T. G. Hornby, D. D. Campbell, J. H. Kahn, T. Demott, J. L. Moore, and H. R. Roth, “Enhanced gait-related improvements after therapist- versus robotic-assisted locomotor training in subjects with chronic stroke: A randomized controlled study,” *Stroke*, vol. 39, no. 6, pp. 1786–1792, 2008.

[43] A. Duschau-Wicke, J. Von Zitzewitz, A. Caprez, L. Lünenburger, and R. Riener, “Path control: A method for patient-cooperative robot-aided gait rehabilitation,” *IEEE Trans. Neural Syst. Rehabil. Eng.*, vol. 18, no. 1, pp. 38–48, 2010.

[44] R. Riener, L. Lünenburger, S. Jezernik, M. Anderschitz, G. Colombo, and V. Dietz, “Patient-cooperative strategies for robot-aided treadmill training: First experimental results,” *IEEE Trans. Neural Syst. Rehabil. Eng.*, vol. 13, no. 3, pp. 380–394, 2005.

[45] D. Aoyagi, W. E. Ichinose, S. J. Harkema, D. J. Reinkensmeyer, and J. E.

Bobrow, “A robot and control algorithm that can synchronously assist in naturalistic motion during body-weight-supported gait training following neurologic injury,” *IEEE Trans. Neural Syst. Rehabil. Eng.*, vol. 15, no. 1, pp. 387–400, 2007.

[46] L. L. Cai *et al.*, “Implications of assist-as-needed robotic step training after a complete spinal cord injury on intrinsic strategies of motor learning.,” *J. Neurosci.*, vol. 26, no. 41, pp. 10564–10568, 2006.

[47] I. Schwartz *et al.*, “The Effectiveness of Locomotor Therapy Using Robotic-Assisted Gait Training in Subacute Stroke Patients: A Randomized Controlled Trial,” *Pm&R*, vol. 1, no. 6, pp. 516–523, 2009.

[48] D. J. Reinkensmeyer *et al.*, “Tools for understanding and optimizing robotic gait training.,” *J. Rehabil. Res. Dev.*, vol. 43, no. 5, pp. 657–670, 2006.

[49] J. L. Emken, J. E. Bobrow, and D. J. Reinkensmeyer, “Robotic movement training as an optimization problem: Designing a controller that assists only as needed,” *Proc. 2005 IEEE 9th Int. Conf. Rehabil. Robot.*, vol. 2005, pp. 307–312, 2005.

[50] R. Banz, M. Bolliger, G. Colombo, V. Dietz, and L. Lünenburger, “Computerized visual feedback: an adjunct to robotic-assisted gait training.,” *Phys. Ther.*, vol. 88, no. 10, pp. 1135–45, 2008.

[51] M. Wellner, A. Duschau-Wicke, J. Von Zitzewitz, and R. Riener, “Stepping over virtual obstacles with an actuated gait orthosis,” in *Proceedings - IEEE Virtual Reality*, 2007, pp. 275–276.

[52] “BAMA Technology - RoboGait.” [Online]. Available: http://www.bamateknoloji.com/en/. [Accessed: 23-May-2017].

[53] S. K. Agrawal, S. K. Banala, and A. Fattah, “A Gravity Balancing Passive Exoskeleton for the Human Leg,” *Robot. Sci. Syst.*, no. 302, 2006.

[54] S. K. Banala, S. K. Agrawal, and J. P. Scholz, “Active Leg Exoskeleton (ALEX) for gait rehabilitation of motor-impaired patients,” in *2007 IEEE 10th International Conference on Rehabilitation Robotics, ICORR’07*, 2007, pp. 401–407.

[55] J. F. Veneman, R. Kruidhof, E. E. G. Hekman, R. Ekkelenkamp, E. H. F. Van Asseldonk, and H. Van Der Kooij, “Design and Evaluation of the LOPES Exoskeleton Robot for Interactive Gait Rehabilitation,” *IEEE Trans. NEURAL Syst. Rehabil. Eng.*, vol. 15, no. 3, 2007.

[56] J. C. P. Ibarra and A. A. G. Siqueira, “Impedance Control of Rehabilitation Robots for Lower Limbs, Review,” in *2014 Joint Conference on Robotics: SBR-LARS Robotics Symposium and Robocontrol*, 2014, pp. 235–240.

[57] R. Steger, S. H. Kim, and H. Kazerooni, “Control scheme and networked control architecture for the Berkeley Lower Extremity Exoskeleton (BLEEX),” in *Proceedings - IEEE International Conference on Robotics and Automation*, 2006, vol. 2006, pp. 3469–3476.

[58] G. Aguirre-Ollinger, “Exoskeleton control for lower-extremity assistance based on adaptive frequency oscillators: Adaptation of muscle activation and movement frequency,” *Proc. Inst. Mech. Eng. Part H J. Eng. Med.*, vol. 229, no. 1, pp. 52–68, 2015.

[59] A. J. Del-Ama, Á. Gil-Agudo, J. L. Pons, and J. C. Moreno, “Hybrid FES-robot cooperative control of ambulatory gait rehabilitation exoskeleton.”

[60] N. G. Tsagarakis and D. G. Caldwell, “Development and control of a ‘soft-actuated’ exoskeleton for use in physiotherapy and training,” *Auton. Robots*, vol. 15, no. 1, pp. 21–33, 2003.

[61] M. Dzahir and S. Yamamoto, “Recent Trends in Lower-Limb Robotic Rehabilitation Orthosis: Control Scheme and Strategy for Pneumatic Muscle Actuated Gait Trainers,” *Robotics*, vol. 3, no. 2, pp. 120–148, 2014.

[62] R. Ekkelenkamp, P. Veltink, S. Stramigioli, and H. Van Der Kooij, “Evaluation of a virtual model control for the selective support of gait functions using an exoskeleton,” in *2007 IEEE 10th International Conference on Rehabilitation Robotics, ICORR’07*, 2007, pp. 693–699.

[63] E. Rocon, J. M. Belda-Lois, A. F. Ruiz, M. Manto, J. C. Moreno, and J. L. Pons, “Design and validation of a rehabilitation robotic exoskeleton for tremor assessment and suppression,” *IEEE Trans. Neural Syst. Rehabil. Eng.*, vol. 15, no. 1, pp. 367–378, Sep. 2007.

[64] K. Kong, H. Moon, D. Jeon, and M. Tomizuka, “Control of an exoskeleton for realization of aquatic therapy effects,” *IEEE/ASME Trans. Mechatronics*, vol. 15, no. 2, pp. 191–200, 2010.

[65] K. Kong, H. Moon, B. Hwang, D. Jeon, and M. Tomizuka, “Robotic rehabilitation treatments: Realization of aquatic therapy effects in exoskeleton systems,” *Proc. - IEEE Int. Conf. Robot. Autom.*, vol. 1, pp. 1923–1928, 2009.

[66] T. Miyoshi, K. Hiramatsu, S.-I. Yamamoto, K. Nakazawa, and M. Akai, “Robotic gait trainer in water: Development of an underwater gait-training orthosis,” *Disabil. Rehabil.*, vol. 30, no. 2, pp. 81–87, 2008.

[67] R. Rupp, P. E. P. Hofer, and D. M. Knestel, “MotionTherapy @ Home – a novel device for automated home locomotion therapy,” pp. 1–4, 2005.

[68] S. Patil, N. Steklov, W. D. Bugbee, T. Goldberg, C. W. Colwell, and D. D. D’Lima, “Anti-gravity treadmills are effective in reducing knee forces,” *J.*

Orthop. Res., vol. 31, no. 5, pp. 672–679, 2013.

[69] "Andago® - Hocoma." [Online]. Available: https://www.hocoma.com/solutions/andago/. [Accessed: 14-May-2017].

[70] M. Saunders, V. Inman, and H. Eberhart, "The major determinant in normal and pathological gait," *J. Bones Jt. Surg.*, vol. 35, no. 3, pp. 543–558, 1953.

[71] M. P. Julius and Zelnik, *Human Dimension & Interior Space: A Source Book of Design Reference Standards*. New York: Watson-Guptill Publications, 1979.

[72] D. H. Sutherland, L. Cooper, and D. Daniel, "The role of the ankle plantar flexors in normal walking.," *J. Bone Joint Surg. Am.*, vol. 62, no. 3, pp. 354–63, Apr. 1980.

[73] B. R. Munson, T. H. (Theodore H. Okiishi, and W. W. Huebsch, *Fundamentals of fluid mechanics*, 6th ed. J. Wiley & Sons, 2009.

[74] T. E. Ertop, T. Yuksel, and E. Konukseven, "Simulation of Fluid Environment using a Robotic Orthosis on Human Lower Extremity for Therapeutic Purposes," *Proc. - Annu. Int. Conf. IEEE Eng. Med. Biol. Soc.*, pp. 5015–5018, 2016.

[75] K. Kong and M. Tomizuka, "Smooth and continuous human gait phase detection based on foot pressure patterns," *Proc. - IEEE Int. Conf. Robot. Autom.*, pp. 3678–3683, 2008.

[76] A. Mansfield and G. M. Lyons, "The use of accelerometry to detect heel contact events for use as a sensor in FES assisted walking," *Med. Eng. Phys.*, vol. 25, no. 10, p. 879, 2003.

[77] K. Tong and M. H. Granat, "A practical gait analysis system using gyroscopes," *Med. Eng. Phys.*, vol. 21, no. 2, pp. 87–94, 1999.

[78] I. P. I. Pappas, M. R. Popovic, T. Keller, V. Dietz, and M. Morari, "A reliable gait phase detection system," *IEEE Trans. Neural Syst. Rehabil. Eng.*, vol. 9, no. 2, pp. 113–125, 2001.

[79] A. Boschmann, P. Kaufmann, and M. Platzner, "Accurate gait phase detection using surface electromyographic signals and support vector machines," *IEEE Intl. Conf. Bioinforma. Biomed. Technol.*, vol. 13, no. 14, p. 15, 2011.

[80] R. R. Neptune, S. A. Kautz, and F. E. Zajac, "Contributions of the individual ankle plantar flexors to support, forward progression and swing initiation during walking," *J. Biomech.*, vol. 34, no. 11, pp. 1387–1398, 2001.

[81] E. Ayyappa, "Normal human locomotion, Part 1: basic concepts and terminology," *J. Prosthetics Orthot.*, vol. 9, no. 1, pp. 10–17, 1997.

[82] T. Bober, K. Kulig, and J. M. Burnfield, “Predictive torque equations for joints of the extremities,” *Acta Bioeng. Biomech.*, vol. 4, no. 2, pp. 49–61, 2002.

[83] A. M. F. Barela, S. F. Stolf, and M. Duarte, “Biomechanical characteristics of adults walking in shallow water and on land.,” *J. Electromyogr. Kinesiol.*, vol. 16, no. 3, pp. 250–6, Jun. 2006.

[84] S. E. Lord and L. Rochester, “Measurement of community ambulation after stroke: Current status and future developments,” *Stroke*, vol. 36, no. 7, pp. 1457–1461, 2005.

APPENDICES

APPENDIX A

PSEUDOCODES FOR COMPUTER SIMULATIONS

1. Single Lower Extremity Computer Simulation

```
density=998.6;
Cd=0.4;

%Velocity Inputs
U_flow=[0 0 0]; %m/s
Ubody=[0 0 0]; %m/s in +y direction.

% Subject Information
SubjectBodyDimensions = importdata('SubjectNo1.xlsx');

% time variable
time=stepsize:stepsize:numbcycles*exercise_Period;

%Angle constants
time_const_hip= 2*pi/exercise_Period;
A_hip= -30; %in degrees
kneeAngle=0; %in degrees
kneeAngVel_Relative=0; % in deg/s

%Loop starts
Foreach t in time

   % Angler calculations
   ang_hip=deg2rad(dot(A_hip,cos(time_const_hip*t) ) );
   ang_knee=deg2rad(kneeAngle);

   %Angular Velocities
   w_hip=deg2rad(dot(A_hip.*(-time_const_hip),sin(time_const_hip*t) ) );
   w_knee=w_hip-deg2rad(kneeAngVel_Relative);
```

```
    %Single Extremity Analysis
    kneeCapVel=Ubody+crossProduct(w_hip, kneeCapPositionVector);

    %Body Segment Force & Moment Calculations
    Foreach bodySegment in [leg, thigh]
        [DragForce(bodysegment), DragMoment(bodysegment)]=DragEffectsCalculator
        (ang_bodysegment, w_bodysegment, jointVel_bodysegment,
        SubjectBodyDimensions.bodysegment, density, Cd, U_flow);
        [BuoyForce(bodysegment), BuoyMoment(bodysegment)]=BuoyancyEffectsCalculator(
        SubjectBodyDimensions.bodysegment, ang_bodysegment, density);
    end

    %Torques at the joints
    Foreach Joint in [knee, hip]
        DragForceActing(Joint) = DragForceActing(PrevJoint)+DragForce(Joint);
        DragTorqueActing(Joint) = DragTorqueActing(PrevJoint) + DragMoment(Joint) +
        crossProduct(PrevJointPositionVector, DragForceActing(PrevJoint) );
        BuoyancyForceActing(bodysegment) = BuoyancyForceActing(PrevJoint) +
        BuoyForce(Joint);
        BuoyancyTorqueActing(Joint) = BuoyancyTorqueActing(PrevJoint) +
        BuoyMoment(Joint) + crossProduct(PrevJointPositionVector,
        BuoyancyForceActing(PrevJoint) );
    end
end %end of the main foreach loop

% Graphs at the end
Plot(time,[angles, angularSpeeds, DragTorquesActing, BuoyancyTorquesActing]);
end
```

2. Full Gait Computer Simulation

```
density=998.6;
Cd=0.4;
fluidLevel=1.3; %m

% Velocity Inputs
vel=0.8; %km/h
Ubody=[0 1 0]*(vel/3.6); %m/s in +y direction
U_flow=[0 0 0]; %m/s

% Enum for Right and Left
R=1; L=2;

% Subject Information
SubjectBodyDimensions = importdata('SubjectNo1.xlsx');

% Reference Gait Data
[ang_hip, ang_knee, w_hip, w_knee, time] = importdata('RefGait.xlsx');

% Loop starts
Foreach t in time

    % Single Extremity Analysis
    Foreach extremity in [Right, Left]
        kneeCapVel(extremity) = Ubody+crossProduct(w_hip(extremity),
        kneeCapPositionVector(extremity) );
```

```
  end
  % Animation
  if animation
    X=[0 kneeCap.x heel.x Toe.x]; %Positions of joints
    Y=-[0 kneeCap.y heel.y Toe.y];
    plot(X, Y);
    pause(t-t_prev);
  end
  % Gait Phase Detection
  [alpha(R) alpha(L)] = SupportAndSwingTransitionAlgorithm(heel(R).y, heel(L).y);
  % Body Segment Force & Moment Calculations
  Foreach bodySegment in [R_leg, R_thigh, L_leg, L_thigh]
    [DragForce(bodysegment), DragMoment(bodysegment)]=DragEffectsCalculator (
    ang_bodysegment, w_bodysegment, jointVel_bodysegment,
    SubjectBodyDimensions.bodysegment, density, Cd, U_flow);
    [BuoyForce(bodysegment), BuoyMoment(bodysegment)]=BuoyancyEffectsCalculator(
    SubjectBodyDimensions.bodysegment, ang_bodysegment, density);
  end
  % Torques at the joints assuming them in Support and Swing Phases
  Foreach Joint in [R_knee, R_hip, L_hip, L_knee] for Left Support & [L_knee, L_hip,
    R_hip, R_knee] for Right Support
    DragForceActing(Joint) = DragForceActing(PrevJoint)+DragForce(Joint);
    DragTorqueActing(Joint) = DragTorqueActing(PrevJoint) + DragMoment(Joint) +
    crossProduct(PrevJointPositionVector, DragForceActing(PrevJoint) );
    BuoyancyForceActing(bodysegment) = BuoyancyForceActing(PrevJoint) +
    BuoyForce(Joint);
    BuoyancyTorqueActing(Joint) = BuoyancyTorqueActing(PrevJoint) +
    BuoyMoment(Joint) + crossProduct(PrevJointPositionVector,
    BuoyancyForceActing(PrevJoint) );
  end
  % Torques at the joints
  Foreach extremity in [R, L]
    Foreach Joint in [knee, hip]
      DragTorques(extremity,Joint) = alpha(extremity) *
      DragTorqueActing_Support(extremity,Joint) + (1- alpha(extremity)) *
      DragTorqueActing_Swing(extremity,Joint);
      BuoyancyTorques(extremity,Joint) = alpha(extremity) *
      BuoyancyTorqueActing_Support(extremity,Joint)+ (1- alpha(extremity)) *
      BuoyancyTorqueActing_Swing(extremity,Joint);
    end
  end
end %end of the main foreach loop
% Graphs at the end
Plot(time,[angles, angularSpeeds, DragTorques, BuoyancyTorques]);
end
```

3. Buoyancy Function for A Single Body Segment

```
function BuoyancyEffectsCalculator(SegmentDimensions, angle, fluidDensity)

% Volume Calculation
Vol=VolumeOfTruncatedCone(SegmentDimensions);

% Valumetric Center Distance
rv_cv = VolumetricCenterOfTruncatedCone(SegmentDimensions, angle);

% Buoyant Force
Force=[-1 0 0]*(Vol*fluidDensity*gravitationalAccel);

% Buoyant Moment
Moment= cross(rv_cv,Force);
return Force, Moment;

end
```

4. Drag Function for A Single Body Segment

```
function DragEffectsCalculator (angle, angularSpeed, jointVel, SegmentDimensions,
fluidDensity, dragCoef, U_flow)

% Relative Velocity Calculations
v(L) = jointVel + angularSpeed * L;
v_rel(L)= v(L) - U_flow;

% Integration for Force & Moment
LimbLenght= SegmentDimensions.Lenght;
Width(L) = SegmentDimensions.WidthProfile;
Force=-(1/2)*fluidDensity*dragCoef* (Integral[0, LimbLenght] ( dotProduct(Width(L) *
UnitNormalVector(angle), v_rel(L) ) * v_rel(L) ) );
Moment=-(1/2)*fluidDensity*dragCoef* (Integral[0, LimbLenght] ( dotProduct(Width(L) *
UnitNormalVector(angle), v_rel(L) ) * crossProduct( stripPosition(L), v_rel(L) ) ) );
return Force, Moment;

end
```

APPENDIX B

THE EXPERIMENTAL FLOW USED FOR COMPLETE GAIT EXPERIMENTS

There exists 4 different experimental work for this study and they are:

- Step Detection
- Land vs Water
- Fluid Parameter Change Effects
- Flow Speed effects

***** HIGHLIGHT EVERY ITEM ON THE LIST WITH GREEN WHEN THEY ARE FINISHED. *****

In this section we will go over the experimental preparation procedures.

1) Informing the subject
    a. Give the participation form to the subject and explain the study briefly
    b. Make the subject to read the form carefully and sign it.
    c. Date =
2) Collect patient data and fill below.
    a. Name=
    b. Adult or Child=
    c. Patient or Healthy=
    d. Gender=
    e. Age=
    f. Weight=
    g. Overall body Length=
3) Measure body Lengths
    a. Lower Extremity
        i. Hip joint to Knee joint Distance, Lk_h=
        ii. Knee joint to Heel Bottom Distance, Lheel_h=
        iii. Distance from Heel to Toe, Ltoe_heel =
        iv. Upper Perimeter Hip=
        v. Lower Perimeter Hip=
        vi. Upper Perimeter Knee=
        vii. Lower Perimeter Knee=
    b. Upper Body

i. **Torso width =**
ii. **Torso Depth=**
iii. **Arm Length=**
iv. **Arm Perimeter=**

Put Input all of the parameters to code as defined variables.

4) Perform referencing action (homing) for the RoboGait.
5) Control the behavior of the robot. Both in Land and Fluid conditions.
6) Selecting correct apparatus to connect the subject to the RoboGait.
   a. **Harness Size=**
   b. **Leg holders Size (From hip to ankle) = [, ,]**
   c. **Feet Tensors Size =**
   d. **RoboGait Tibia Length =**

   After all apparatus is selected connect the subject to the RoboGait.

   a. **Positon of Leg holders at Sagittal Plane (From hip to ankle) = [, ,]**
   b. **Positon of Leg holders at Coronal (Frontal) Plane (From hip to ankle) = [, ,]**
7) Make dry runs to allow the subject to get familiar with the setup.
8) Step Detection Exp.
   a. Only apply Compensation Torques. (Fluid Model Torques are **OFF**)
   b. Make Counter weight on the crane 0 kg. And make sure that the subject has enough distance to travel with the Body Weight Support System (BWSS) for natural up-and-down movement
   c. Set **Walking Speed to +0.6 km/h**.
   d. Ask ready to Subject. Start the walk when ready.
   e. **Start taking a HIGH Speed Video, File Name =**
   f. When treadmill speed becomes stable, set **the Walking speed to +0.8 km/h.**
   g. Let the subject walk undisturbed for **3 mins**.
   h. Terminate the walk. Enter a text to the log as "**SubjectNo-StepDetectionExp**"
   i. Name of the data log file for Step Detection =
9) Land vs Water Exp.
   a. Land
      i. Only apply Compensation Torques. (Fluid Model Torques are **OFF**)
      ii. Make Counter weight on the crane 0 kg. And make sure that the subject has enough distance to travel with the Body Weight Support System (BWSS) for natural up-and-down movement
      iii. Set **Walking Speed to +1.0 km/h**.
      iv. Ask ready to Subject. Start the walk when ready.
      v. When treadmill speed becomes stable, adjust **the Walking speed** according to the subject. The Walking Speed should be just below the subject's comfort level. When selected, keep the Walking Speed constant.
      vi. The Selected Land Walking Speed =
      vii. Let the subject walk undisturbed for **6 mins**.
      viii. Terminate the walk. Enter a text to the log as "**SubjectNo-LandvsWaterExp-LandCond-WalkingSpeed**"
      ix. **Name of the data log file for Land=**
   b. Water
      i. Apply Fluid Model Torques. (Fluid Model Torques are **ON**)
      ii. Set the fluid model parameters to **density 998.6 kg/m3 , Circular Drag Coef=0.4 , Fluid Level 1.3 m , Flow Velocity [0 0 0] km/h (Default values)**
      iii. Calculate the total buoyancy on the body
      iv. Check Total Buoyancy and Patient Weight ratio

v. Make Counter weight on the crane equal total buoyancy of the body in kg. And make sure that the subject has enough distance to travel with the Body Weight Support System (BWSS) for natural up-and-down movement
vi. **Counter weight on the crane=**
vii. Set **Walking Speed to +0.8 km/h**.
viii. Ask ready to Subject. Start the walk when ready.
ix. When treadmill speed becomes stable, adjust **the Walking speed** according to the subject. The Walking Speed should be just below the subject's comfort level. When selected, keep the Walking Speed constant.
x. **The Selected Water Walking Speed =**
xi. Let the subject walk undisturbed for **6 mins**.
xii. Terminate the walk. Enter a text to the log as "**SubjectNo-LandvsWaterExp-WaterCond-WalkingSpeed**"
xiii. **Name of the data log file for Water=**

10) Flow Velocity Exp

a. Base Line
i. Apply Fluid Model Torques. (Keep Fluid model torques ON)
ii. Set the fluid model parameters to **density 998.6 kg/m3 , Circular Drag Coef=0.4 , Fluid Level 1.3 m , Flow Velocity [0 0 0] km/h**
iii. Calculate the total buoyancy on the body
iv. Make Counter weight on the crane equal total buoyancy of the body in kg. And make sure that the subject has enough distance to travel with the Body Weight Support System (BWSS) for natural up-and-down movement
v. **Counter weight on the crane=**
vi. Set **Walking Speed to +0.8 km/h**.
vii. Ask ready to Subject. Start the walk when ready.
viii. When treadmill speed becomes stable, set **the Walking speed to +1.0 km/h**
ix. Let the subject walk undisturbed for **4 mins**.

b. Walking in downstream direction (Flow is the same direction with the walking direction, "+" Flow speed)
i. Keep the subject walking
ii. Set the fluid model parameters to **Flow Velocity [0 +0.8 0] km/h (in the form [x y z]) and do not change anything else**
iii. **Counter weight on the crane= The same with Flow Baseline Walking**
iv. Let the subject walk undisturbed for **6 mins**.

c. Walking in Upstream direction (Flow is the opposite direction with the walking direction, "-" Flow speed)
i. Keep the subject walking
ii. Set the fluid model parameters to **Flow Velocity [0 -0.8 0] km/h (in the form [x y z]) and do not change anything else**
iii. **Counter weight on the crane= The same with Flow Baseline Walking**
iv. Let the subject walk undisturbed for **6 mins**.
v. Terminate the walk. Enter a text to the log as "**SubjectNo-FlowExp**"
vi. **Name of the data log file for Flow Exp.=**

11) Parameter Effects Exp

a. Base Line
i. Apply Fluid Model Torques. (Keep Fluid model torques ON)
ii. Set the fluid model parameters to **density 998.6 kg/m3 , Circular Drag Coef=0.4 , Fluid Level 1.3 m , Flow Velocity [0 0 0] km/h**
iii. Calculate the total buoyancy on the body

iv. Make Counter weight on the crane equal total buoyancy of the body in kg. And make sure that the subject has enough distance to travel with the Body Weight Support System (BWSS) for natural up-and-down movement
v. **Counter weight on the crane=**
vi. Set **Walking Speed to +0.8 km/h**.
vii. Ask ready to Subject. Start the walk when ready.
viii. When treadmill speed becomes stable, set **the Walking speed to +1.0 km/h**
ix. Let the subject walk undisturbed for **4 mins**.
x. Terminate the walk. Enter a text to the log as "**SubjectNo-ParamExp-Baseline**"
xi. **Name of the data log file for Baseline Case=**

b. High Drag Case
i. Apply Fluid Model Torques. (Keep Fluid model torques ON)
ii. Set the fluid model parameters to **density 998.6 kg/m3 , Circular Drag Coef=1.0 , Fluid Level 1.3 m , Flow Velocity [0 0 0] km/h**
iii. Calculate the total buoyancy on the body
iv. Make Counter weight on the crane equal total buoyancy of the body in kg. And make sure that the subject has enough distance to travel with the Body Weight Support System (BWSS) for natural up-and-down movement
v. **Counter weight on the crane=**
vi. Set **Walking Speed to +0.8 km/h**.
vii. Ask ready to Subject. Start the walk when ready.
viii. When treadmill speed becomes stable, set **the Walking speed to +1.0 km/h**
ix. Let the subject walk undisturbed for **6 mins**.
x. Terminate the walk. Enter a text to the log as "**SubjectNo-ParamExp-HighDrag**"
xi. **Name of the data log file for High Drag Case=**

c. Low Fluid Level Case
i. Apply Fluid Model Torques. (Keep Fluid model torques ON)
ii. Set the fluid model parameters to **density 998.6 kg/m3 , Circular Drag Coef=0.4 , Fluid Level 1.0 m, Flow Velocity [0 0 0] km/h**
iii. Calculate the total buoyancy on the body
iv. Close the software and open crane control.
v. Make Counter weight on the crane equal total buoyancy of the body in kg. And make sure that the subject has enough distance to travel with the Body Weight Support System (BWSS) for natural up-and-down movement
vi. Close Crane control and Run our software.
vii. **Reenter all parameters** and Calculate the total buoyancy and check.
viii. **Counter weight on the crane=**
ix. Set **Walking Speed to +0.8 km/h**.
x. Ask ready to Subject. Start the walk when ready.
xi. When treadmill speed becomes stable, set **the Walking speed to +1.0 km/h**
xii. Let the subject walk undisturbed for **6 mins**.
xiii. Terminate the walk. Enter a text to the log as "**SubjectNo-ParamExp-LowFluidLevel**"
xiv. **Name of the data log file for Lower Fluid Level Case=**

d. High Fluid Density Case
i. Apply Fluid Model Torques. (Keep Fluid model torques ON)
ii. Set the fluid model parameters to **density 1200.0 kg/m3 , Circular Drag Coef=0.4 , Fluid Level 1.3 m, Flow Velocity [0 0 0] km/h**
iii. Calculate the total buoyancy on the body
iv. Close the software and open crane control.

v. Make Counter weight on the crane equal total buoyancy of the body in kg. And make sure that the subject has enough distance to travel with the Body Weight Support System (BWSS) for natural up-and-down movement
vi. Close Crane control and Run our software.
vii. **Reenter all parameters** and Calculate the total buoyancy and check.
viii. **Counter weight on the crane=**
ix. Set **Walking Speed to +0.8 km/h**.
x. Ask ready to Subject. Start the walk when ready.
xi. When treadmill speed becomes stable, set **the Walking speed to +1.0 km/h**
xii. Let the subject walk undisturbed for **6 mins**.
xiii. Terminate the walk. Enter a text to the log as "**SubjectNo-ParamExp-HighDensity**"
xiv. **Name of the data log file for Higher Density Case=**